Dear Editor,

We kindly thank the reviewers for their comments and will address each reviewer's comments separately. Where orthographic errors or changes in sentence structure have been suggested, we have changed spelling and, in some cases, structure. Therefore to keep this reply clutter-free we will only address those reviewer comments that pertain to the scientific content.

Firstly, we shall address the review of Jacques Précigout, presenting first the reviewer's comment and then the corresponding reply. Thereafter, we will address the comments of Luiz F.G. Morales.

Please find a copy of the revised manuscript below the authors replies with the pertinent changes highlighted.

Best,

James Gilgannon

Reviewer 1: Jacques Précigout

COMMENTS ON TEXT:

Page 1-abstract: The object and techniques used have to be summarised in the abstract. In its present form, we have no idea of what the authors did.

We have expanded the abstract to more specifically state the objective and techniques used.

P3-L27: More information about the thicknesses of carbon coating have to be given here. Actually, in an ideal case, it is not recommended to use carbon coating for EBSD analyses, but sometimes, it is better to add a few nanometers to avoid ≪charging≫ effect. So what thickness did you put on your sample block ?

We have added the thickness of the carbon and gold coatings to the manuscript.

P5-L10: Please add the reference of Bachmann et al. (2010) for MTEX

We appreciate the reviewer's direction on this matter but our citation choice for MTEX was made based on the guidance provided on the MTEX website (http://mtex-toolbox.github.io/publications.html). Here it is stated, "...please cite one of the following paper that best fits your application.". From the selection provided we chose Mainprice *et al.* (2011) because of its focus on deformation mechanisms and rheology. As the authors of MTEX have not specified a specific citation requirement we will retain our choice but thank the reviewer for his suggestion.

P5-L11: Some precisions are here required concerning the minimum number of indexed points per grain. Is that in one row, several rows or for the whole grain? We commonly use a minimum threshold of 5 consecutive pixels in several rows.

In our case it was a filtering condition of 10 indexed points per whole grain. We have amended the text accordingly.

P9-L1: The figure 6d is called before figure 6b. Please, make sure that the figures are properly called in the manuscript (in successive order).

We have corrected this mistake and now call figures in successive order.

P10-L23: The figure 9a is not called anywhere.

Figure 9 a is now called in the text (Note that figure 9 is now figure 10 in the manuscript).

P11-L20: Please add the reference of Kassner and Hayes (2003) after ≪dislocations≫.

We are aware of the work of Kassner and Hayes (2003) but feel that the inclusion of this work does not add to the literature already cited. Through out the manuscript we cite directly literature that the Kassner and Hayes (2003) review paper draws on. This choice was deliberate to provide a direct link to specifically relevant papers for each statement. We provide the relevant citations after the next, more specific, sentence.

P13-L29: It would be interesting to discuss our paper here (Précigout et al., 2017, Nature communications), which deals with the relationships between creep cavitation and phase nucleation in ultramylonites. The authors also have to discuss the recent paper of Cross and Skemer (2017, JGR solid Earth). Moreover, I have a question about your sentence claiming that fluid-filled cavities remain unfilled: if phase nucleation does not arise from creep cavitation, how do you explain the transition from GSI to GSS creep by phase mixing? In our paper in 2016 (Précigout and Stünitz, 2016), we do not claim that phase nucleation necessarily follows cavitation. We just say that phase nucleation is fast enough to maintain grain size small and randomize the olivine fabric. Some cavities may remain unfilled, particularly if the fluid is undersaturated.

The reviewer raises several points with in his comment and we will address each point separately.

- *It would be interesting to discuss our paper here (Précigout et al., 2017, Nature communications), which deals with the relationships between creep cavitation and phase nucleation in ultramylonites.*

  We thank the reviewer for pointing us towards his contribution. At the time of writing our manuscript the first author had not read the work of Précigout *et al.* (2017) and so it was not included in the discussion. Précigout *et al.* (2017) presents compelling results, primarily from olivine slip systems and hydrous phase distributions, as evidence for fluid circulation in mantle rocks. While the results of this study are of interest to the topic of strain localisation and phase mixing at large, Précigout *et al.* (2017) do not present results that pertain to the processes of creep cavitation. Précigout *et al.* (2017) assume that cavities become active in their model but provide little direct evidence of creep cavities, or of a time evolution of phase mixing. Therefore while we appreciate the reviewer's suggestion we think that the discussion of the results of our study does not necessitate the inclusion of a discussion of Précigout *et al.* (2017). We have, however, amended the introduction to include a citation of Précigout *et al.* (2017) as a work that invokes creep cavities in their study.

- *The authors also have to discuss the recent paper of Cross and Skemer (2017, JGR solid Earth).*

  The reason for the exclusion of the paper from the discussion is that we wished to address the questions around the process of creep cavities explicitly, and we feel that the contribution of Cross and Skemer (2017) does not address this but targets more broad continuum mechanical questions of rheological weakening. While we agree that their contribution is a valuable one to the topic of localisation and rheology, their discussion focuses heavily on what they call "geometric phase mixing" which in simpler terms is the development of banding or compositional stratification. In terms of rheology, they discuss how this "geometric phase mixing" can contribute to mechanical weakening. However, the formation of compositional bands is not phase mixing *sensu stricto*. Their discussion focuses on what can be considered as a form of higher order clustering, something like Thomas clustering (Wiegand and Moloney, 2013). Our work focuses on the microstructures akin to the tail end of their experiments, the dispersal of monomineralic domains, or the development of anti-clustering. These results in the work of Cross and Skemer (2017) are given little attention in their discussion. Hence we feel that the work of Cross and Skemer (2017) does not present results that warrant discussion in the context of our results.

- *Moreover, I have a question about your sentence claiming that fluid-filled cavities remain unfilled: if phase nucleation does not arise from creep cavitation, how do you explain the transition from GSI to GSS creep by phase mixing? In our paper in 2016 (Précigout and Stünitz, 2016), we do not claim that phase nucleation necessarily follows cavitation. We just say that phase nucleation is fast enough to maintain grain size small and randomize the olivine fabric. Some cavities may remain unfilled, particularly if the fluid is undersaturated.*

  The question of phase mixing does not need to be restricted to two solid phases but can be extended to a solid-fluid system. Our rational behind this statement is as follows:

  1. If, as we speculate, the Zener-Stroh mechanism arises out of a creeping monomineralic quartz domain to provide sites of dilation, then there is a now a way to introduce a distributed second, fluid, phase into a single phase domain.
  2. In addition to this, fluid contributes to the continuum mechanical properties of the rock. A fluid filled pore would achieve this at the grain scale by acting to inhibit grain boundary migration and grain growth.

3. Furthermore, cavities that open will act as sites of low stress, encouraging the infiltration of a fluid. This can lower the adhesion and cohesion of grain boundaries, locally enhancing grain boundary sliding.
4. The final consequence of introducing creep cavities is that, even in the absence of solid phase precipitates, is that they perturb a homogenous domain into a two-phase rheological system.

COMMENTS ON FIGURES:

Figure 1: Giving the GPS point is not enough, the authors have to provide a simplified map of Australia that locates the sample area. I would also recommend to add a picture of the outcrop. The figure 1C is not located. The figure 1B is not labelled.

Our contribution focuses on understanding the evolution of processes active at the micro scale and therefore we feel that adding a map and field photo does not enhance the manuscript or that these form a necessary step in following the main arguments. We have provided several relevant references for the Redback Shear Zone if the reader wishes to gain further insight to the sample's field context.

Figure 2 (caption): I think it is ≪figure 2e and f≫, not ≪figure 2e and d≫.

We have changed the caption accordingly.

Figures 6 and 7: these two figures arrive too late in the manuscript. They should appear after figure 1, particularly to show the microstructural features of pores. The text will have to be changed accordingly. By the way, the figure 1C has to be shown with figure 6. The figure 7 also demonstrates that the authors documents 3D features coeval with rock deformation. It has to be given before going into details concerning the distribution and shape of micro-cavities.

The reviewer raises several points with in his comment and we will address each point separately.

- *Figures 6 and 7: these two figures arrive too late in the manuscript. They should appear after figure 1, particularly to show the microstructural features of pores. The text will have to be changed accordingly.*

  We thank the reviewer for this suggestion, however, after much consideration we feel that we disagree. While we see the value in presenting the conventional microstructural images together and early, in the manuscript we frame the contribution around key quantitative results that drive the conceptual model. In this sense the observations in figure 6 on the broken surface are qualitative and supportive of the quantitative image analysis in the XZ plane. Furthermore due to the difficulties in processing the nCT data set no quantitative insights, with reasonable uncertainties, could be presented other than the connectivity. Therefore figure 7 is also mostly supportive of the observations in the XZ plane. We do concede that the results could be rearranged but we do not see any greater benefit to restructuring the manuscript so significantly.

- *By the way, the figure 1C has to be shown with figure 6.*

  In line with our response above, we feel we disagree with the addition of figure 1c to figure 6, primarily because the figure is constructed with reference to observations in one plane of finite strain. We do not wish to confuse the reader by mixing planes of observation within a figure. However, we have added a clearer cross reference between figure 6b and 1c to draw the readers eye to similarities of pore shapes observed.

- *The figure 7 also demonstrates that the authors documents 3D features coeval with rock deformation. It has to be given before going into details concerning the distribution and shape of micro-cavities.*

  We do not agree that Figure 7 alone documents the porosities coeval activity with rock deformation. On its own figure 7 shows that the porosity is pervasive and connects in 3D. It is the complete and contextualized set of observations presented in the paper that provides insight into when the pores were most likely active. In fact the two strongest lines of evidence are the change in pore shape congruent with the changes in microstructure and the corresponding changes in grain misorientation. Therefore we would argue, as above, that figure 7 is mostly supportive and there is not an obvious benefit to moving the figure.

Figure 6 (caption): please details the sub-figures (a, b, c, etc.). I am not sure that the figure 6e is necessary.

Some details of sub-figures have been added to the caption.

Figure 8: The EBSD maps have to be shown in the manuscript (not in supplementary material), at least to show the sub-grains. I would recommend to show the three of them. Furthermore, the c axes have to be spelled between square brackets (≪ [0001] ≫) and the <a> axes are commonly indicated using <11-20>. The pole figure texture is based on, but not the ODF. Please change ≪ ODF ≫ by ≪ texture ≫ (or equivalent). Please provide the Mindex, as well. That will definitely confirm your point about the distribution of misorientation angles. Use ≪ uniform ≫ instead of ≪ random ≫ in the figure legend.

The reviewer raises several points, we will address them separately:

- *The EBSD maps have to be shown in the manuscript (not in supplementary material), at least to show the sub-grains. I would recommend to show the three of them.*

  As advised we have moved the EBSD maps into the manuscript proper.

- *Furthermore, the c axes have to be spelled between square brackets (≪ [0001] ≫) and the <a> axes are commonly indicated using <11-20>.*

  We have changed the c-axis to be indicated with square brackets and we have changed the <a> family to the convention indicated by the reviewer.

- *The pole figure texture is based on, but not the ODF. Please change ≪ ODF ≫ by ≪ texture ≫ (or equivalent).*

  We have retained the label of ODF because it is the ODF that is displayed. We calculate the ODF and then display it in a pole figure. Therefore it is the ODF calculation that we are in fact visualising. We do not wish to mislead the reader into thinking that it is contoured point data we present.

- *Please provide the Mindex, as well. That will definitely confirm your point about the distribution of misorientation angles.*

  We see no need to present the M-index as we already present misorientation angle histograms for each subset. Furthermore the relative change in the J-index with the changing microstructure already validates, with an independent method, the changes seen between the misorientation angle histograms. Presenting the M-index calculation is therefore unnecessary.

- *Use ≪ uniform ≫ instead of ≪ random ≫ in the figure legend.*

  We have changed random to uniform in the figure legend.

References:

Wiegand, T. and Moloney, K. A. (2013). Handbook of Spatial Point-Pattern Analysis in Ecology. 1: Chapman and Hall/CRC.

Reviewer 2: Luiz F.G. Morales

COMMENTS ON TEXT:

1) Although I like the idea of Zener-Stroh cracking mechanism to explain the initial porosity in the quartz rich bands, the evidence provided is not totally convincing because of the lack of TEM analyses in the studied sample. The TEM imaging in this case is really necessary because one has to be able to see the dislocations aligned against some sort of "barrier" (a grain boundary, or particular slip plane), where they would piled up and eventually coalesce to form voids and cracks. This is obviously not very easy but would be a more convincing evidence for the activation of this mechanism during the deformation of the quartz bands and the cavities. The *authors also have to keep in mind that in quartz one will be never sure if the dislocations pile up to form the porosity of if the porosity (and the stress concentration around it) will be the place where the dislocations are nucleated, because we cannot see dislocations moving. Another possible way to tackle better this problem would evolve, for instance, the detailed EBSD mapping around the pores to see if there any evidence of more distorted lattice around the voids or somewhere in the grains;*

We agree that TEM imaging is really required to categorically place the Zener-Stroh mechanism as the cavity nucleating mechanism. Unfortunately, this project lacked the resources to explore our samples with this technique. However, we would like to pursue TEM work on these samples in future. With respect to detailed EBSD mapping, this is an excellent idea and we attempted this but it was found to be exceptionally difficult to identify the smallest cavities and surrounding grains with the necessary precision. As to the argument of a lacking direct evidence we have been careful to make clear that we speculate on the nucleation mechanism. For the most part we tried to focus on discussing the consequences of having cavities nucleate in a monomineralic domain that creeps by dislocation creep. The exact nucleation mechanism must arise from a scenario where its domain of origin is compositionally homogenous and has a mechanical restriction with respect to the amount of angular momentum of grains.

2) The authors mentioned that roughly the porosity is generated in grain boundaries aligned with the YZ plane of finite strain. From the graphics of Fig. 3, the predominant porosity shape is rather irregular, and although there is a predominance of porosity long axes parallel to Z (Fig. 3a), I did not understand the relation to Y, considering that the analyses were performed in the XZ section. Maybe there is some piece of information missing about the calculation of the Y-axis (for instance, as a cross-product of the long and short axes extracted from the maps). Or maybe the authors should include analysis in an orthogonal section?

The reference to the Y direction of finite strain comes from qualitative observations on the broken surface. It is observed that elliptical pores sit on grain boundaries that are aligned with the Y direction of finite strain (e.g. fig. 6e upper left white arrow). In figure 6a there is a qualitative insight into all three principle directions of finite strain as the broken surface drops away from the YX surface of the image giving a view into the Z direction as well. The combination of this, and other images, allowed us to assess that many of the elliptical pores existed on grain boundaries roughly aligned with the YZ plane of finite strain.

3) In the section 4.5 the authors say that they have clear evidence for "subgrains and lattice distortions", but this is not evident in the figures. For instance the misorientation angle histogram in the Figs. 8a and 8b do not show a low angle misorientation peak as one would expect when quartz is deformed in the crystal plasticity field. I guess this is related to the cut off misorientation angle chosen for the grain calculations in MTEX, so the authors have to provide new histograms where these peaks are more clear. This is also necessary because the EBSD map in the supplementary material does not show abundant subgrain boundaries.

4) A very interesting feature in these misorientation histograms is the lack of a misorientation peak at 60 °, related to Dauphine twinning. Do the authors "cleaned" the twinning or the lack of twins is a real feature in this sample. If the later is the case, this should be discussed in the paper, as this is not very common in quartz EBSD data;

We shall treat comments 3) and 4) together as they are related:

The reviewer correctly assesses that we only presented grain misorientations in figure 8's misorientation angle histograms. We filter out the subgrains and the Dauphine twinning peak at 60 ° misorientation. In the revised version, we have amended the figure to explicitly state that the misorientation angle histograms only contain grain boundary misorientaitons. We do not wish to include the subgrains and the Dauphine twinning in the misorientation angle histograms as we aim to show how grain boundary misorientations change with the microstructure. Furthermore, while we agree that even after filtering one should expect a low angle misorientation peak for a domain deforming by the crystal plasticity, our microstructure shows an already perturbed system, as evidenced by the presence of cavities. This makes it unlikely that such a strong low angle misorientation peak will be seen compared to a domain without cavities, where fluids have not infiltrated and grain boundary strengths have not been weakened allowing rotations.

We disagree with the reviewer's comment about the lack of evidence for subgrains and lattice distortions. The largest grains found in supplementary figure 2 (now figure 8 of the manuscript) show subgrain walls developed. Furthermore, in supplementary figure 2b (now figure 8b of the manuscript) pixels are coloured for their misorientation with respect to the mean orientation of the grain that hosts them and it can be seen that many of the largest grains show a gradient in misorientation. This suggests that the lattices in these grains are distorted. To be clear we do not claim that the map shows excessive subgrains or that all grain lattices are distorted.

Page 2: Line 3-4 – I would briefly discuss these three different models like in two sentences each, that allows a quick comparison between models;

We have amended the text accordingly.

Line 16 – is there any temperature estimation for the deformation?

There is a temperature estimation provided but the way we structured the sentence it may not have been clear. The temperature has been better highlighted in the text.

Page 4: equation 1 (and the others) – is there any reference for these equations, like Heilbronner's book?

We have found a reference for equation 1 but not for equation 2. We have cited the Fiji reference again for equation 2.

Page 5: line 6 – please add where the EBSD data was acquired (Bern?);

We have added the location of data acquisition.

Line 10 – Mainprice et al. is not the correct reference for MTEX, the correct is Hielscher & Schaeben 2008 - A novel pole figure inversion method: specification of the MTEX algorithm, J. of Appl. Cryst., 41(6), 2008.

As previously discussed in reviewer 1's comments we appreciate the reviewers' direction on the appropriate citation. However, our citation choice for MTEX was made based on the guidance provided on the MTEX website (http://mtex-toolbox.github.io/publications.html). Here it is stated, "...please cite one of the following paper that best fits your application.". From the selection provided we chose Mainprice *et al.* (2011) because of its focus on deformation mechanisms and rheology. As the authors of MTEX have not specified a specific citation requirement we will retain our choice but thank the reviewer for his suggestion.

Line 11 – please specify the parameters for the ODF calculations (halfwidth, etc). This is given in the figures but should be included here

We have added the parameters for the ODF calculations.

Line 23 – what do you mean by thin section wafer?

We were referring a thin-section and have removed the word 'wafer'.

Line 20 – how calcic is the plagioclase? Please give an estimative of An content

We thank the reviewer for asking because we mistakenly suggested the plagioclase was more calcic. In fact the plagioclase has an An content of $\sim 28\%$, making the plagioclase much more sodic than calcic. We have changed the text to reflect this.

Page 7, line 6 – please briefly explain how the hexbin statistic works;
Line 15 – how do you define high and low beta angles?

We have added a brief explanation of hexbin plots to the methods (3.3.1 Image analysis). An explanation of the definition of beta is given in the methods too (3.3.1 Image analysis: Pore orientation).

4.2.4 – the numerical definitions in the figure are different from the ones presented in the text

We have amended this discrepancy.

Line 17 – the authors mentioned 3 clusters, but I only see one, maybe the authors should indicate them in the figures;

As we do not wish to crowd the figure with extra annotations, we point to the clusters by coordinate position of the figure in the caption.

Line 8 – the authors mentioned that the dentrites are Si-rich. Looking at their Fig. 6, it is clear that the dentrites have a maximum of few 100's of nanometers in thickness. If the EDS was done with 20 kV as mentioned in the paper, the volume of interaction in quartz would be around 1 μm, meaning that the Si X-ray signal the authors detected may come from the quartz underneath. Did the authors performed low kV EDS analyses for better spatial resolution (less interaction volume)?

Unfortunately, we did not. However, we compensated for the larger interaction volume by increasing the aperture size and lengthening the count time. Reducing the interaction volume might possibly yield slightly different results but we consider this unlikely. Reducing the interaction volume would just change the ratio of counts between the quartz below and the surface itself. We feel that by counting for longer and thereby increasing the ability to catch more x-rays with an increased aperture compensated enough for a rough characterisation.

Page 11, line 30 – dominant slip. . .plane? Direction?

We have added direction to the text.

Line 13, line 9-10 – in the way is written, it reads as if the fluids could induce pinning

This is how we meant it to sound. Fluids are known to inhibit grain boundary mobility (see discussion of Reviewer 1's comments above). In our case, as in the case with a solid second phase, the dragging energy will compete with the surface energy to slow or inhibit grain boundary migration.

COMMENTS ON FIGURES:

General comment – either rotate all the pictures to have foliation E-W compatible with the pole figures in Fig. 8 (and the standard tectonic reference frame with foliation/lineation E-W) or rotate the pole figures from figure 8 to have the foliation N-S

We have rotated the figures to the standard tectonic reference frame with foliation/lineation E-W and have changed the text accordingly.

Figure 1 – you should separate A, and C from the big picture B, and also write B on the big picture. You should also consider making A and C bigger, in the printed version the features are really small (consider also increasing the font size)

We have revised figure 1 to better highlight the features.

Figure 2 & 3 – I would make all the pictures bigger

The figure sizes here reflect the Latex formatting. We have designed the figures so that they should be legible on a portrait A4 page.

Figure 4 – The authors mentioned in the caption that the largest pores have high beta values (with long axes parallel to X) but this is not clear from the Fig. 4b, there are only 7 or 9 points with blue colors (indicating larger pores) with high beta values, is this number relevant, considering that for intermediate size pores (yellow) you have much more points covering a full range of beta values?

We agree that the largest pores with the closest alignment to X are debatably relevant. They are potentially cracks that run parallel to the foliation and it is difficult to determine their genetic origin (i.e. post or synkinematic). However from figures 3b and c we know that there seems to be a continuum, defined by a power law relationship, between the intermediate pores and the largest pores. With this in mind suggest that it is hard to rule out the relevance of the small population of large pores aligned to X, primarily because the very nature of a power law relation dictates that there will be a small number of larger pores. Most of our line of discussion later does not focus on this small population of larger pores but we have added a note in the text to highlight the point that the reviewer raised.

Figure 5 – please make the scale for A & C and B & D the same, for easier comparison

We have set the scales to the same values and provided additional kernel density plots to verify the changes we claim occur with true point density analysis. We have added additional information in both the methods and supplementary material sections to describe the parameters used in the kernel density analysis.

Figure 6 – in the picture D you point to "incipient precipitates" (I imagine you are refer- ring to the brig tiny spots), but the tip of your arrow points to an artefact caused by the grains from the coating, you should move the arrow to point exactly one of the bright spots or make a circle around the whole area

We have implemented the change suggested by the reviewer.

Figure 7 – Is there a colorcode for the 3D model of porosity? And is it possible to have the same orientation as X-Y-Z as in the 2D figures?

We have clarified the colour coding in the figure caption. Unfortunately we only know the sample's reference to the foliation plane. Therefore as we cannot decompose the foliation plane into X and Y, we cannot accurately provide a reference to the principle axes of finite strain. We have instead given reference in the caption to the figure's relationship to the foliation plane.

Figure 8 – your contoured pole figures are missing the primitive circle of the stereonet. The arrows pointing to quartz grain dispersion and quartz domain width should be more separate and the font larger. The font needs to be larger in the pole figure legend and in the histograms. Pleas also write [0001] instead of (0001).

We have implemented the changes requested by the reviewer.

Hierarchical creep cavity formation in an ultramylonite and implications for phase mixing

James Gilgannon[1,2], Florian Fusseis[2], Luca Menegon[3], Klaus Regenauer-Lieb[4], and Jim Buckman[5]

[1]Institute of Geological Sciences, University of Bern, Baltzerstrasse 1+3, CH-3012 Bern, Switzerland
[2]School of Geosciences, The University of Edinburgh, Grant Institute, Edinburgh EH9 3JW, UK
[3]School of Geography, Earth and Environmental Sciences, Plymouth University, Plymouth PL4 8AA, UK
[4]School of Petroleum Engineering, The University of New South Wales, Kensington NSW 2033, Australia
[5]Institute of Petroleum Engineering, Heriot-Watt University, Edinburgh EH14 4AS, UK

Correspondence to: J. Gilgannon (james.gilgannon@geo.unibe.ch)

Abstract. Establishing models for the formation of well mixed polyphase domains in ultramylonites is difficult because the effects of large strains and thermo-hydro-chemo-mechanical feedbacks can obscure the transient phenomena that may be responsible for domain production. We use scanning electron microscopy and nanotomography to offer critical insights into how the microstructure of a highly deformed quartzo-feldspathic ultramylonite evolved. The dispersal of monomineralic quartz domains in the ultramylonite is interpreted to be the result of the emergence of syn-kinematic pores, called creep cavities. The cavities can be considered the product of two distinct mechanisms that formed hierarchically: Zener-Stroh cracking and viscous grain boundary sliding. In initially thick and coherent quartz ribbons deforming by grain size-insensitive creep, cavities were generated by the Zener-Stroh mechanism on grain-boundaries aligned with the YZ plane of finite strain. The opening of creep cavities promoted the ingress of fluids to sites of low stress. The local addition of a fluid lowered the adhesion and cohesion of grain-boundaries and promoted viscous grain boundary sliding. With the increased contribution of viscous grain boundary sliding, a second population of cavities formed to accommodate strain incompatibilities. Ultimately, the emergence of creep cavities is interpreted to be responsible for the transition of quartz domains from a grain size-insensitive, to a grain size-sensitive rheology.

1 Introduction

Microstructural observations of shear zones in nature and experimental investigations of monomineralic systems in the laboratory have demonstrated that the evolution of a ductile fault rock through the mylonite series can entail a switch from a dislocation creep-controlled (grain size-insensitive (GSI)) to a diffusion creep-controlled (grain size-sensitive (GSS)) bulk rheology (e.g. Etheridge and Wilkie, 1979; Poirier, 1980; Kilian et al., 2011). In quartzo-feldspathic rocks at mid-crustal conditions, this progressive evolution often leads to the development of distinct microstructural elements in close spatiotemporal proximity: feldspathic porphyroclasts, monomineralic quartz bands and well mixed, fine-grained, polyphase domains (fig. 1). Each of these elements have been shown to accommodate deformation differently, e.g. feldspars fracture and react, quartz experiences GSI creep while the polyphase domains deform by GSS processes (Mitra, 1978; Kerrich et al., 1980; Behrmann and Mainprice, 1987; Fliervoet et al., 1997; Stipp et al., 2002; Tullis, 2002). Generally speaking, with ongoing deformation the proportion of fine-grained material deforming by GSS creep increases syn-kinematically, so that the polyphase domains form an interconnected weak layering. It is the establishment of these well mixed, anti-clustered polyphase domains that is recognised to ultimately promote a switch in the bulk rheology of the rock (Handy, 1994; Kilian et al., 2011; Herwegh et al., 2014). However, the exact modes by which these domains are established are still poorly understood and the subject of intense research.

One of the details under investigation is the role of fluids and their pathways. Models have been proposed for brittle fracture based pumping and advection of fluids (Etheridge et al., 1984), diffusion dominated granular flow (Paterson, 1995) and more recently a *dynamic granular fluid pump* that is dominated by fluid advection (Fusseis et al., 2009). Fusseis et al. (2009) postulated that in ultramylonites, fine-grained polyphase domains deforming by viscous grain boundary sliding (VGBS) develop the *dynamic granular fluid pump*. This pump operates during deformation and utilizes a syn-kinematic porosity known as creep cavitation. Here, creep cavitation is defined as a porosity that results from entropy production during deformation. A stringent consequence of this definition is that pore nucleation must arise directly out of the active deformation mechanism's response to the shortening and stretching of the rock mass. It is clear that a model generating fluid pathways in the middle crust that does not require brittle fracturing has significant implications for the controls of the exchange of fluids between the hydrostatic and lithostatic pore fluid pressure regimes (Ingebritsen and Manning, 2010), phase nucleation in mylonites (Kruse and Stünitz, 1999) and by extention, rheology.

The phenomenon of creep cavitation has been well described in material science, with several distinct types of creep cavitation being distinguished (Riedel, 1987). To date, geological research has identified evidence for creep cavitation in natural ultramylonites from the middle crust (Behrmann and Mainprice, 1987; Mancktelow et al., 1998; Herwegh and Jenni, 2001; Fusseis et al., 2009; Kilian et al., 2011; Rogowitz et al., 2016) and the lower crust (Závada et al., 2007; Menegon et al., 2015), as well as in mantle rocks (Rovetta et al., 1986; Précigout et al., 2017). Experimental work has shown that octachloropropane, quartzite, diabase, feldspar aggregates, anorthite-diopside aggregates, olivine-clinopyroxene aggregates and calcite-muscovite aggregates can develop creep cavities (Caristan, 1982; Hirth and Tullis, 1989; Ree, 1994; Dimanov et al., 2007; Rybacki et al., 2008; Delle Piane et al., 2009; Précigout and Stünitz, 2016). This data set is small but diverse and suggests that creep cavities can occur in many types of deforming rocks across varying pressure, temperature and rate conditions.

The wide variety of metamorphic conditions at which cavities form suggests that a range of micro-scale processes contribute to creep cavitation. Many of the geological works cited interpret that creep cavities are the product of VGBS and form to accommodate strain incompatibilities (Behrmann and Mainprice, 1987; Ree, 1994; Herwegh and Jenni, 2001; Dimanov et al., 2007; Závada et al., 2007; Rybacki et al., 2008; Fusseis et al., 2009; Kilian et al., 2011; Menegon et al., 2015; Précigout and Stünitz, 2016). In the VGBS-based model of Fusseis et al. (2009), cavitation at some grain triple junction is balanced by cavity closure on others. This dynamic model of cavity formation is limited to domains deforming by some form of diffusion creep, and does not account for all reports of creep cavities in geology. In other studies, creep cavitation was linked to the production of crystal defects (Wong, 1990; Rogowitz et al., 2016). It is unclear how these mechanisms relate to each other across rock types or if it is possible for multiple cavitation mechanisms to be active simultaneously.

Despite a growing body of observations on creep cavitation in rocks, some important open questions remain, including:

(i) How do creep cavities effect an evolving rock rheology and how does this ultimately influence rock deformation?

(ii) How ubiquitous are creep cavities in deformed rocks and what combination of deformational processes facilitate their formation?

This contribution addresses question (i) by examining in detail the nature and occurrence of creep cavities in a mid-crustal ultramylonite from the Redbank Shear Zone (Australia), and furthers our understanding of question (ii). We use a sophisticated workflow combining electron microscopy, image analysis, electron back-scatter diffraction (EBSD) and synchrotron-based x-ray nanotomography (nCT) to show that creep cavities can form by multiple mechanisms in one sample. We present a high-resolution map of porosity distribution on the mm scale in an ultramylonite and demonstrate how this porosity evolved during mylonitic deformation.

2 Geological setting and sample description

The Redbank Shear Zone (RBSZ) is part of a crustal scale thrust duplex that formed during the Alice Springs orogeny in Central Australia (Teyssier, 1985b). Due to its geometry, where higher-grade shear zones piggy-backed on lower-grade shear zones, the RBSZ has experienced no significant retrograde metamorphic overprint during its exhumation, and the syn-kinematic mineral fabrics and parageneses are preserved (Fliervoet et al., 1997). Micro-fabrics in the RBSZ are therefore ideal for the investigation of transient chemo-physical processes that characterise mid-crustal shear zones.

The RBSZ is a network of shear zones that cascades across scales, with shear zone thicknesses that range from 10^{-3} to 10^{1} m, displaying a characteristic protomylonite - mylonite - ultramylonite succession (Teyssier, 1985a). This contribution focusses on a quartzo-feldspathic ultramylonite sampled from the amphibolite facies shear zones in the Black Hill area of the RBSZ (Sample BH02, 23°32’46.81"S, 133°25’14.42"E; temperature, 350-550 °C; lithostatic pressure, 500 MPa, (Fliervoet et al., 1997)). The sample is a banded ultramylonite that displays a striking and extensive grain-boundary porosity that is hosted in fine grained ($\sim< 20$ μm), monomineralic, quartz bands (fig. 1). In addition, the sample shows thick domains of well-mixed polyphase material as well as a network of fine-grained ($\sim 1 - 2$ μm) polyphase layers that envelop large, fractured augen porphyroclasts (~ 1 mm). In general, the sample’s foliation is defined by the monomineralic quartz bands and the thicker polyphase domains, whereby the quartz bands display no signs of boudinage. This work focusses on the microstructure of the quartz bands and the nature of the porosity they host. We interpret the disaggregating quartz domains at different stages of dispersal (cf. Kilian et al., 2011) to offer an insight into the locally evolving quartz micro-fabric and an associated porosity.

3 Methods

3.1 Sample Preparation

We analysed a small sample block, which was cut parallel to the stretching lineation and perpendicular to the foliation (long and short axis dimensions of sample: 22.9/19.4 mm) and then polished and carbon-coated (thickness ~ 20 nm) for electron microscopy and EBSD. To split the sample along the mylonitic foliation (after electron microscopy), it was pre-cut parallel to the stretching lineation and cleaved in a vice. The split surface was gold-coated (thickness ~ 3 nm).

3.2 Data Acquisition and Processing

3.3 Microstructural Analysis

A large (41448 x 40282 pixel, at a scale of 1:35.5 ($px : nm$)) back-scatter electron (BSE) map was acquired on a FEI Quanta FEG 650 SEM operated at an accelerating voltage of 20 kV. This map was stitched from individual images using the Maps software by FEI.

3.3.1 Image analysis

The BSE map formed the basis of a detailed analysis of porosity. In BSE images, pores appear black. They were segmented using binary thresholding and labelled in Fiji (Schindelin et al., 2012) after a pre-processing workflow was applied to reduce noise (see supplementary material). Data were visualised with Matplotlib Python libraries (Hunter, 2007). Hexbin plots were used to help visualise large data scatter plots. A hexbin plot works by laying a hexagon grid over the data and then preforming a chosen operation on the data within the bounds of each hexagon. An example of operations that can be performed on data with in a hexagon include; count, sum and calculate the mean. The *Kernel density* for point features in ESRI's ArcGIS v10.1 software was used in pore cluster analysis for figure 2. The kernel smoothing factor was automatically calculated with reference to the population size and extent of analysis and contoured based on a $1/4\sigma$ kernel. For figure 5 kernel density calculations where made using the SciPy (Jones et al., 2001–) and NumPy (van der Walt et al., 2011) Python libraries (see supplementary material for parameters used).

From the segmented data, the following parameters were evaluated:

– **Pore size**

Defined as the cross-sectional area (in μm^2) of a pore.

– **Pore orientation**

Pore orientations were determined by using the long axis of the best fit ellipse and calculating its deviation from the vertical axis of images shown. For ease of viewing, the orientation measures were folded along their symmetry axis, 90°, and presented as the value β . For example, $\beta = 0°$ describes a long axis aligned parallel to the vertical axis of the image analysed (and orthogonal to the mylonitic foliation in fig. 1) and $\beta = 90°$ would be orthogonal to this (and parallel to the mylonitic foliation).

- **Pore shape descriptions**

$$Circularity = \frac{4\pi\,(Pore\,area)}{(Pore\,perimeter)^2} \tag{1}$$

Circularity is a shape descriptor that quantifies the complexity of a shape by linking the area and perimeter. It is important to note that circularity values are not unique but simply describe a deviation in shape from the area and perimeter relationship of a circle. A circularity value of 1 describes such a circle and decreasing values can represent either an increase in shape complexity (e.g. a star) or shape elongation, or a combination of both (Cox, 1927).

$$Roundness = \frac{4\,(Pore\,area)}{\pi\,(Major\,axis)^2} \tag{2}$$

Roundness is a shape descriptor that only quantifies elongation. Used together, circularity and roundness can characterise pore shape complexity and elongation more correctly (Schindelin et al., 2012).

3.4 Electron backscatter diffraction, EBSD

EBSD data were collected at Bern University on a Zeiss Evo 50 SEM equipped with a Digiview II camera. The sample was tilted to 70°, and a 20 kV accelerating voltage applied [beam current was ≈2.5 nA, working distance ≈11.5 mm]. Crystallographic orientation data were obtained with a 0.65 μm step size from automatically indexed EBSD patterns in TSL OIM. EBSD data were processed and plotted with MTEX (Mainprice et al., 2011). Raw data points with $<$0.1 confidence index (CI) and calculated grains with $<$10 indexed points in total were excluded from analysis. Orientation distribution functions (ODF) calculated for pole figures use a kernel half-width of 7°, while ODFs calculated for misorientation angle histograms use a kernel half-width of 5°.

3.5 Split sample

Broken surfaces, explored in the SEM, provide insight into pore morphologies and evidence for redistribution of material (cf. Mancktelow et al., 1998; Fusseis et al., 2009). Images from the split sample were acquired on a Carl Zeiss SIGMA HD VP FEG SEM using a 20 kV accelerating voltage and a ∼6.5 mm working distance. Oxford AZtecEnergy energy dispersive X-ray (EDX) analysis was conducted at an aperture setting of 60 μm and used to qualitatively evaluate phase compositions on the split surface. This form of mineral identification was necessary to interpret individual pores in their microstructural context.

3.6 X-ray nanotomography

We used an Xradia synchrotron-based nanotomograph at the Advanced Photon Source (beam line APS/32-ID) to acquire 3-dimensional nanotomographic datasets of porous ultramylonitic quartz ribbon bands and assess the potential interconnectivity of pores. A cylindrical sample (20 μm diameter x 100 μm length) was extracted using focussed ion beam techniques from a polished thin section that was cut from the sample. In the tomograph, radiographic projections were acquired over a rotation of 180° at 8 keV beam energy and reconstructed to yield a 3-dimensional nanotomographic dataset with a spatial resolution in the order of 70 nm. Porosity was segmented with binary thresholding and labelled in Avizo Fire. Due to the small sample size and the noisiness of the data, no quantitative analysis was attempted. Volumetric data were visualised in Avizo.

4 Result

4.1 Micro-fabric domains

The investigated high strain micro-fabric is composed of four microstructural components (fig. 1):

(1) Monomineralic quartz domains are elongated parallel to the foliation, exhibiting a varying degree of coherency as domains. Here coherency is used in the context of the quartz grains spatial distribution, to describe qualitatively the degree to which quartz grains are aggregated into monomineralic bands vs. dispersed into segregated grains. The most coherent quartz domains wrap around porphyroclasts and in some cases mantled pophyroclasts. The fringes of the thickest quartz domains show evidence for the removal of individual quartz grains and their progressive assimilation into neighbouring, poorly mixed polyphase domains. We assume that thinner quartz domains have advanced further on the path of disaggregating and that the progression from thicker to thinner quartz domains reflects a progressive microstructural evolution. This assumption does not presuppose that all thin quartz domains where once very thick, but we consider it highly unlikely that any thin quartz ribbon was initially just one or two grains (of a 10 - 20 μm diameter) wide (fig. 1).

(2) Porosity that can be considered tri-modal: pores on quartz grain boundaries, pores hosted within porphyroclasts, and cracks that cross cut and run parallel to the foliation. Feldspar porphyroclasts host an intra-crystalline, angular porosity, which is distinctly different from the inter-crystalline porosity observed in association with quartz (see detailed discussion below).

(3) Well-mixed and poorly-mixed polyphase domains: The finest-grained ($<$ 1-2 μm) parts of the ultramylonite make up the well-mixed polyphase domains (see left-hand side of fig. 1a). There also exist less well-mixed polyphase domains which contain disaggregated quartz ($<$ 10 μm) (fig. 1b and c). The polyphase domains comprises plagioclase, K-feldspar, mica, epidote, ilmenite and quartz (fig. 1c).

(4) Porphyroclasts, which are generally either sodic plagioclase or K-feldspar. The K-feldspar porphyroclasts occasionally display flame perthites. Sodic oligoclase plagioclase porphyroclasts exhibit what appears to be reaction to fine-grained mantles of K-feldspar and mica (fig. 1). No quartz porphyroclasts are observed.

4.2 Image analysis in the XZ plane of finite strain

Pores were analysed in a representative area (2.1 mm^2) of the sample. Figure. 1b shows the full extent of the area used for both spatial and pore shape analysis. Areas for subset analysis are also marked in figure 1b. Pores in all domains were extracted and considered in bulk for density analysis. Subsequently, masks were applied to quantify total porosity and analysing pore shapes in quartz domains separate from porphyroclasts and the polyphase domains. Pores in porhyproclasts and the fine-grained polyphase domains were analysed together.

4.2.1 Spatial distributions of pores

Kernel density analysis demonstrates that the porosity is anisotropically distributed, with a bimodal clustering in respect to domains (figs. 2c and d). The majority of observable pores (86%) exist in direct spatial association with quartz ribbon bands. In quartz domains, the highest density is recorded in the thickest, most coherent ribbons. In the porphyroclast and polyphase domains, the larger feldspar porphyroclasts that have seen the least fracture or reaction to smaller components show the highest density of pores. The total porosity measured in the area shown in figures 2e and f is presented in table 1.

4.2.2 Pores in monomineralic quartz

Segmented pores were analysed to identify any systematic changes in pore size, shape and orientation. Figures 3 and 4 show the analysis for the area shown in figure 1b, while figure 5 shows the subset analyses.

4.2.3 Pore sizes

It can be seen that pores cover a limited range of values in cross-sectional area (focused strongly around a median value of 0.18 μm^2) but vary greatly in long axis orientation (fig. 3a). The lower limit of pore area may be controlled by the resolution of the imaging technique. At first inspection there are two maxima in figure 3a: Pores with a low β and pores with a high β. The maximum for low β values appears to be more significant.

4.2.4 Pore shapes

As stated above, a pore's shape complexity and elongation can be characterised by combining circularity and roundness. When circularity is plotted against roundness, three salient clusters are observed (fig. 3b):

1. Pores with a circular character ($circularity \approx 1, roundness \approx 1$)
2. Pores with an elliptic character ($circularity \approx 1, roundness \approx 0.8$)
3. Pores with a complex shape but only moderate elongation ($circularity \approx 0.3, roundness \approx 0.8$)

Figure 3c shows that when area is plotted against perimeter and coloured for circularity, there are some systematics that can be described by two power law relationships:

$$Area = 0.062 * Perimeter^{1.498} \quad (3)$$

$$Area = 0.072 * Perimeter^{1.081} \quad (4)$$

We assign pores described by these equations to two distinct populations. From figure 3, it is evident that the pores characterised by equation 3 have very high circularity. Furthermore, figures 3b and c suggest that the very circular pores are the smallest (in cross-sectional area). These small, circular pores are then linked by equation 3 to the elliptical pores (elliptical pores having a $circularity \approx 0.8, roundness \approx 0.8$). This relation can be most clearly seen in fig. 3c, where equation 3 describes pores of a circularity ranging from 1 to ≈ 0.75. Similarly, equation 4 suggests that all pores with circularity values below ~ 0.8 are systematically linked and scale in shape with a power law relationship.

4.2.5 Changes in pore orientations

We assume that the long axis of a pore's best fit ellipse is roughly parallel to the orientation of the pore's boundary with the host minerals, and therefore representative of pore orientation. For pores with a circularity less than 1, the Feret diameter is seen to have the same orientation as the long axis of the best fit ellipse (see supplementary fig. 1). Figure 3a shows a variation in pore orientations but does not readily highlight any systematics. However, if figure 3a is considered with figure 3c, it can be seen that pores whose shape is governed by equation 3 generally have a lower value of β (see pores with areas $\sim \leq 0.1\ \mu m^2$). Figure 4 decomposes this observation to show clearly that orientations of the more circular pores (> 0.8) rarely exceed $45°$, and predominately assume a low angle to the Z direction of finite strain (fig. 4a). The change in pore orientation at a circularity of 0.8 corresponds to the change in the equation governing pore shape (see fig. 3c). There is also a clear propensity for the largest, least circular pores ($> 2\ \mu m^2$) to be oriented more parallel to the shear plane (fig. 4b). It is unclear if these largest pores are foliation parallel cracks that post date deformation.

4.2.6 Porosity with a changing quartz microstructure

Spatial analysis of pore occurrences has already shown that pore density decreases with quartz domain thickness (fig. 2d). In combination with microstructural evidence for the disaggregation of quartz domains it is possible to consider the evolution of porosity congruent with that of quartz domains (fig. 5). It can be observed that the pore shape descriptors change with the quartz microstructure. Firstly, in the thicker quartz domain, both pore populations (described in eqs. 3 and 4) are observed (fig. 5c). In this domain, pores generally have their long axes aligned with the Z-direction of finite strain (fig. 5a and b). However, both the pore population and orientation change as quartz domains become thinner. It can be seen that in the thinner quartz domain there is an absence of pores from the trend described by eq. 3 (fig. 5f), and that pore orientations become far more variable (fig. 5d and e).

4.3 Observations of pores in the XY plane of finite strain

4.3.1 Pore shapes and orientations

On the broken surface, the porosity present in the thickest quartz domains shows a clear preference to occur along grain-boundaries roughly parallel to the YZ plane (fig. 6a). When the pore morphology is considered with respect to the grain-boundary arrangement at the pore location, two end-member shapes can be identified. *Firstly* there exist roughly elliptical pores in the YZ plane. These pores can either show an asymmetry, truncating on a flat grain-boundary (e.g. upper most white arrow in fig. 6a), or be symmetrical about the grain boundary (e.g. smaller pore in fig. 6b). *Secondly*, there is an occurrence of angular pores at quartz grain triple junctions (see all yellow arrows in fig. 6).

4.3.2 Precipitates on grain-boundaries

The broken surface also reveals information about material redistribution in spatial association with the porosity in the quartz directly surrounding a plagioclase porphyroclast. The porphyroclast itself shows reaction to more K-rich material, which appears to have a flakey morphology (see the area highlighted as Kfs in fig. 6c). In contrast, nearby quartz grain boundaries are covered in a dendritic material (see lower left-hand side of fig. 6c). The EDX conducted on the broken surface showed the chemistry of the dendrites to be Si-rich, with no other obvious chemical signal. Sharply truncated dendrites (see blue arrow in fig. 6c) seem to preferentially occur on dilatant quartz grain boundaries. Figure 6d highlights textural evidence linking crystallite precipitation (empty blue arrow in fig. 6d) and a dendrite on a dilatant grain-boundary (filled blue arrow in fig. 6d). It is noteworthy that very little evidence for dissolution of quartz can be found. Etch pits were observed only on one site (fig. 6d).

Interestingly, many pores appear empty, but some also seem filled with crystallites. With increasing distance from the porphyroclast there is a transition from the dendritic features on the dilatant grain-boundaries to clusters of crystallites in pores and along grain boundaries (see all blue arrows in fig.6e). At the furthest distances from the porphyroclast, in the quartz domain, only small amounts of very isolated crystallites are observed (fig. 6b).

4.4 Observations of pores in the 3D

Due to a range of technical difficulties, nCT yielded only one dataset that provided insights into a porous quartz layer of about 50 μm width. Figure 7 shows a visualisation of labelled pores and highlights interconnected creep cavities in three dimensions. The pores in this layer are mostly oblate and seem to occupy a range of orientations, mostly at high angles to the foliation (parallel to the top and bottom surfaces of the bounding frame). Most importantly, it is clear from figure 7 that pores are indeed interconnected and not constrained to the polished surface investigated in this study. We consider this proof that at most a small minority of pores observed in figure 1 are formed by plucking during sample preparation.

4.5 EBSD analysis

To better understand any potential link between the porosity and the mechanisms accommodating mylonitic deformation in quartz domains, EBSD analysis was undertaken. The results show clear evidence for crystal plastic processes with the presence of a crystallographic preferred orientation (CPO), sub-grains and the occurrence of lattice distortions (fig. 8 and fig. 9). These crystal plastic processes are not uniform across the area analysed (fig. 8b). It can be seen that the thicker quartz band hosts more features that are considered diagnostic of dislocation creep (fig. 8b and fig. 9 subset 1). These processes then become less well-articulated in the thinner quartz band (fig. 8b and fig. 9, subset 2). The abatement of lattice distortions and subgrains coincides with a reduction in grain size and texture strength. The loss of texture strength in the pole figures is further expressed in the misorientation angle distributions, with the thinner quartz band showing a near uniform distribution of misorientations (fig. 9, subset 3).

5 Discussion

5.1 A model for syn-kinematic creep cavitation by different mechanisms

Our study not only advances our understanding of porosity distribution in mid-crustal ultramylonites but also provides critical insight into the mechanisms behind syn-kinematic cavity formation and the associated effects on rock rheology.

To develop this in detail, we interpret different quartz microstructures in our sample as representing different stages in a progressive evolution ("space for time", (see also Fusseis et al., 2006; Kilian et al., 2011). If the well-mixed polymineralic domains are the most mature parts of the studied ultramylonite, monomineralic quartz domains must be considered as relics of an original mylonitic fabric that has been captured in the process of disaggregation. The mechanisms of disaggregation can be observed at the jagged edges of monomineralic quartz domains as well as by comparison of thinner, less coherent, quartz domains with thicker, more coherent, ones. Our EBSD data from these domains suggest that during progressive disaggregation, quartz micro-fabrics with a clear CPO get randomised (fig. 9). This is typically interpreted as indicating a transition from GSI creep to GSS creep accommodated by viscous grain boundary sliding (Mitra, 1978; Etheridge and Wilkie, 1979; Kerrich et al., 1980; Behrmann and Mainprice, 1987; Závada et al., 2007; Kilian et al., 2011; Herwegh et al., 2014; Menegon et al., 2015; Viegas et al., 2016).

Our data show how a syn-kinematic porosity can be associated with this inferred change in rheology, and the formation of a quartzo-feldspathic ultramylonitic micro-fabric. In our sample, quartz domains are associated with an overt porosity and we consider the pores in the quartz domains to be creep cavities (Riedel, 1987). We claim that the cavities evolved syn-kinematically with both the microstructure and the dominant deformation mechanisms, finding that the disintegration of quartz domains is a result of the emergence of creep cavities. These creep cavites have two distinct populations and formed hierarchically. We integrate our findings in a model (fig. 10) where Zener-Stroh cracking produced small cavities in domains deforming by GSI creep (fig. 10a, blue trend; fig. 10b, Time 1). We infer that their formation promoted fluid ingress, which in turn lowered the adhesion and cohesion of grain boundaries (cf. Billia et al., 2013). The addition of a fluid locally increased the contribution of VGBS to strain energy dissipation, which led to the formation of a second population of creep cavities (fig. 10a, green trend; fig. 10b, Time 2) (Fusseis et al., 2009).

Image analysis constrained the two populations of creep cavities in detail (fig. 3c):

(i) Cavities with a perimeter smaller than about $\sim 2\mu m$ with long axes that have a low angle to the YZ plane of finite strain (figs. 3c and 4a) and are governed by the power law relation in equation 3.

(ii) A population of larger cavities that has initially jagged or incised perimeters and generally elliptic shapes (figs. 3b and c). The long axes of these larger cavities exhibit a wider variation in orientation (fig. 4a). However, the largest of these cavities tend to be aligned with grain boundaries that are parallel to the shear plane (fig. 4b). This population is governed by the power law relation in equation 4.

In our sample, thicker, more coherent quartz domains show more of the former population, and thinner, less coherent quartz domains contain only cavities of the latter characteristics (fig. 5). It can also be observed that congruent with the change in cavity characteristics and domain width, there is a randomisation of the CPO present (fig. 9). We interpret these observations to indicate that larger cavities are associated with VGBS.

Syn-kinematic creep cavitation by VGBS is not a new idea in geology: several microstructural (Behrmann and Mainprice, 1987; Herwegh and Jenni, 2001; Závada et al., 2007; Fusseis et al., 2009; Kilian et al., 2011; Menegon et al., 2015) and experimental works (Ree, 1994; Dimanov et al., 2007; Rybacki et al., 2008; Précigout and Stünitz, 2016) invoke the process. Experimential work by both Dimanov et al. (2007) and Rybacki et al. (2008) show that pores generated during deformation by VGBS have a complex, angular and elongated shape. This agrees well with our observations from increasingly disaggregated, thinner quartz domains (fig. 5, subset 2) with their weakened CPO (fig. 9, subset 2). As this type of cavity formation has been well discussed in previous contributions we will not examine this further.

In some contrast, geological descriptions of creep cavities that formed by Zener-Stroh cracking are still rare (Rogowitz et al., 2016). In quartz domains of our sample that deformed dominantly by GSI creep, the population of very small cavities do not occur at grain triple junctions but rather seem to nucleate along grain-boundaries that are aligned in the YZ plane of finite strain (figs. 4a, 5 (subset 1) and 6, all white arrows). Boundaries in these orientations are mechanically unlikely to experience significant sliding, which suggests that VGBS is not conditional for cavity formation and alternative mechanisms might be relevant. In material science, it has been shown that creep cavities in an environment that is characterised by work hardening can nucleate by the coalescence of dislocations. This will occur where crystallographic slip bands intersect with grain-boundaries or grain-boundary precipitates allowing dislocations to pile up, thus forming Zener-Stroh cracks (Stroh, 1957; Bauer and Wilsdorf, 1973). On the basis of our observations we speculate that cavitation by Zener-Stroh cracking could have provided an initial porosity in monomineralic quartz domains that emerged directly out of GSI creep and potentially played an important role in the rheological evolution of the ultramylonite.

5.2 Nucleation of creep cavities during GSI creep

Despite evidence provided by cavity shapes and orientations (fig. 3,4,5 and 6) unequivocal proof of Zener-Stroh cracking is difficult. For the Zener-Stroh mechanism to act, the material must have an abundance of crystal defects produced by deformational work (Stroh, 1957). In our sample, the presence of a CPO, sub-grains and the occurrence of lattice distortions in the thick quartz domains are evidence for the activity of dislocation creep processes and hence the production of crystal defects in the same microstructural domains that host creep cavities. Our analysis further shows that the orientation of the dominant slip direction in these domains is aligned with the X direction of finite strain (fig. 9, subset 1). Grain-boundaries at high angles to the X direction (i.e. those in the YZ plane) could provide the obstacles required for dislocations to pile up, which could result in cavitation by Zener-Stroh cracking (Stroh, 1957). Evidence for quartz grain-boundary porosity in association with high dislocation density has been reported in previous studies from ultramylonites (Shigematsu et al., 2004; Behrmann, 1985; Rogowitz et al., 2016). Recently, Rogowitz et al. (2016) explicitly invoked the Zener-Stroh mechanism to explain small grain-boundary cavities next to dislocation pile ups. In the light of these studies and despite that fact that we can only provide indirect evidence, its seems reasonable to speculate that the process of cavity nucleation could be that of Zener-Stroh cracking.

A dislocation-driven cavitation would require an appropriate density of dislocations to be present for a creep cavity to nucleate. It follows that cavity production consumes defects, and in this way it is a process that may directly compete with other recovery processes such as sub-grain wall formation. Our SEM observations of cavities and sub-grains suggests that both coexist. Kilian et al. (2011) has demonstrated the importance of sub-grain wall formation in the disaggregation process of quartz domains in quartzo-feldspathic ultramylonites that have experienced similar geological conditions as those investigated here. From an irreversible thermodynamic perspective, integrating cavitation as a dissipative component of dislocation creep would expand our current understanding of a crystal's internal entropy production (see eq. 1 of Huang et al. (2009)). This would alter equation 18 of Huang et al. (2009), which describes the total rate of reduction (ρ^-) of the dislocation density at a steady state (ρ). Integrating Zener-Stroh crack formation as a ρ^- mechanism would yield:

$$\frac{d\rho^-}{\gamma} = \frac{d\rho^-_{DRX}}{\gamma} + \frac{d\rho^-_{DRV}}{\gamma} + \frac{d\rho^-_{CAV}}{\gamma} \tag{5}$$

Where $\frac{d\rho^-_{DRX}}{\gamma}$, $\frac{d\rho^-_{DRV}}{\gamma}$ and $\frac{d\rho^-_{CAV}}{\gamma}$ are the dislocation annihilation rates due to dynamic recrystallisation, dynamic recovery, and creep cavitation respectively.

Rogowitz et al. (2016) have recently demonstrated in a fine-grained calcite ultramylonite ($\sim$3 μm) that recovery can occur without the formation of sub-grain walls. Internal strain is recovered by extensive glide and dislocation networks characteristic of cross-slip and network-assisted dislocation movement. In conjunction with this mechanism, Rogowitz et al. (2016) also observed Zener-Stroh crack formation. This may outline a scenario where cavity production dominates over sub-grain wall formation.

Where we infer Zener-Stroh cracking to be responsible for cavity nucleation, Hippertt (1994) proposed an alternative model to explain a concentration of pores on grain-boundaries at high angles to the fabric attractor in a sheared micaceous quartzite (see fig. 10 in Hippertt (1994)). Hippertt (1994) suggested that the initial porosity is loosely connected to preferential dissolution of quartz at sites where dislocation tangles intersect grain boundaries (cf. Wintsch and Dunning, 1985). In both the sample of this study, and of Hippertt (1994), there is a clear link between the pore orientation and the bulk finite strain. Considering the inferred orientations of compression and extension in our sample, preferential dissolution should be expected orthogonal to the observed cavities (see etch pit formation n fig. 6d), i.e. creep cavities in our sample open at sites that would be favourable for precipitation, not dissolution. We therefore consider the model of Hippertt (1994) as incompatible with our observations.

5.3 The role of creep cavities in the activation of GSS creep

The rheological evolution of mid-crustal ultramylonites to GSS creep is prompted by the establishment of a very fine grain size. In ultramylonites that deform by GSS creep, grain growth is usually inhibited by the presence of secondary phases, a process called Zener pinning (Herwegh et al., 2011). Where syn-kinematic creep cavities control fluid transport in ultramylonites (Fusseis et al., 2009; Menegon et al., 2015), cavities should also control secondary phase precipitation and hence directly influence Zener pinning (Herwegh and Jenni, 2001). This invites a discussion on how creep cavitation could influence Zener pinning and thereby facilitate the transition of a rock's rheology from GSI to GSS creep. A critical step in the rheological evolution of the ultramylonite investigated here is the transition from GSI to GSS creep in disintegrating quartz domains.

Conspicuously, secondary minerals are generally absent in the monomineralic quartz domains. We speculate that fluid-filled creep cavities will have affected grain boundary migration directly by acting as pinning phases, therefore arresting grain sizes at sub-equilibrium dimensions and promoting the transition to VGBS. This idea can be further explored by combining our data with the Zener parameter, which quantifies the influence of second phases on rheology (Herwegh et al., 2011):

$$Z = \frac{d_{sp}}{f_{sp}} \tag{6}$$

where Z is the Zener parameter, d_{sp} is the size and f_{sp} is the volume fraction of the secondary phases. Equations 3 and 4 give an empirical indication into the value of d_{sp} for creep cavitation via Zener-Stroh cracking and VGBS, respectively. The dynamic nature of creep cavitation suggests that d_{sp} is not constant but varies between a maximum and a minimum that can be taken from figure 3a. However it is unclear how f_{sp} would evolve with the different cavity formation mechanisms. Any porosity derived exclusively from dislocation creep would be expected to have a characteristic spacing between pores on a grain-boundary, dictated by the crystal volume and the amount of strain that an individual slip system can accommodate. Therefore in this scenario f_{sp} would be directly linked to this characteristic spacing. On the other hand, values of f_{sp} generated by porosity linked to VGBS would have a different character. The volume fraction in this case may be linked to a space problem, where the amount of dilatancy is limited by the surrounding grains. In either case, cavitation should be considered as mechanism that is capable of evolving the Zener parameter and hence the rheology of a domain from GSI to GSS.

Our model ties in with more recent experimental observations by Précigout and Stünitz (2016), who also identify creep cavitation as a means of producing domains that deform by GSS creep. In contrast to our results, Précigout and Stünitz (2016) discuss the deformation of clinopyroxene embedded in an olivine matrix, where phase mixing occurs in clinopyroxene tails.

This process is interpreted to be initiated by micro-cracking. Précigout and Stünitz (2016) advocate a model where the nucleation rate of secondary phases is high. New phases are precipitated simultaneously with micro-cracking and each new cavitation site becomes filled with new phases, which suppresses the development of a CPO. On the other end of the spectrum, our observations highlight a scenario where the rates of precipitation are so slow that cavities remain fluid-filled. Evidence of quartz precipitation is possibly observed in the form of Si-rich grain boundary features (fig. 6, see all blue arrows), but in our interpretation any precipitation is volumetrically not significant enough to fill cavities. Another major difference between the two models is that our model does not require brittle fractures to initiate the disaggregation of a monomineralic domain. The results of our work probably showcase an example where the nucleation of phases is not kinetically or energetically favourable.

5.4 A lack of boudinage but maintenance of strain compatibility

A striking feature of the ultramylonite is the lack of any evidence for boudinage in quartz layers. This implies that either the syn-kinematic viscosity contrast between the polyphase and the quartz domains was small (Smith, 1975; Viegas et al., 2016), or that the quartz layer was not able to achieve localisation because the local temperature fluxes were efficiently dissipated (Peters et al., 2015). Boudinage by either of these processes is considered a ductile instability, where irrecoverable change occurs and grows over time (cf. Peters et al., 2015). In our sample a syn-kinematic porosity is observed and can be considered itself a ductile instability. As discussed above, creep cavitation by Zener-Stroh would be a dissipative feature of dislocation creep that would act to lower the internal energy of a grain. In thermodynamic terms creep cavities could act as an energy sink. From a micro-mechanical perspective, a syn-kinematic porosity offers the possibly of lowering grain-boundary adhesion and cohesion as fluid is drawn to low stress sites (Fusseis et al., 2009; Billia et al., 2013), thereby compromising the rheological integrity of the monomineralic quartz domains and promoting sliding. Therefore, it may be the case that cavity formation in quartz domains inhibits strain localisation via boundinage and the increase in the contribution of VGBS accommodates the extension of quartz layers, facilitating the quartz bands' ultimate demise.

6 Conclusions and outlook

In this study we utilise a workflow of SEM based techniques and synchrotron x-ray nanotomography to rigorously examine the nature and occurrence of a grain-boundary porosity found in recrystallised quartz ribbons of a quartzo-feldspathic ultramylonite. We find that the porosity developed syn-kinematically from the deformation mechanisms active in quartz and the pores can thus be considered as creep cavities. We propose a model of hierarchical creep cavity formation that has implications for both the mircostructural and rheological maturation of an ultramylonitc fabric. We interpret based on the orientation of creep cavities and the crystallographic texture of quartz domains that Zener-Stroh cracking is responsible for the initial nucleation of creep cavities. The opening of creep cavities promotes the ingress of fluids to sites of low stress, and the local addition of a fluid lowers the adhesion and cohesion of grain-boundaries promoting VGBS. The increased activity of VGBS is documented in the thinning of quartz domains. In thinner quartz domains both the texture weakens and cavities become more complex, eventually elongating. We suggest that cavitation at this stage of the quartz microstructural evolution is governed by VGBS. Zener-Stroh cracking can be directly linked to crystal plasticity, and our observations therefore potentially point to a wider significance of creep cavitation in mylonitic deformation. It remains unclear if the emergence of Zener-Stroh cracking is contingent on quartz becoming the locally stronger phase. This would restrict the model presented here to scenarios where some fine grained mixtures have already emerged. Most importantly our findings document a micro-mechanical path for clustered quartz grains to be dispersed into an well-mixed phase mixture.

Both of the invoked creep cavity formation mechanisms are well known from material sciences and are intimately linked to ductile failure in metals and ceramics (Bauer and Wilsdorf, 1973; Gandhi and Ashby, 1979; Riedel, 1987; Shigematsu et al., 2004). Our model points to the coeval activity of both mechanisms in mid-crustal ultramylonites. This raises questions about how these creep cavities interact? While it is unclear if natural samples can reveal such transient aspects, it is clear that such questions of critical importance in furthering our understanding of mylonitic processes and crustal deformation in general.

Data availability. High resolution BSE image available from J. Gilgannon (james.gilgannon@geo.unibe.ch)

Table 1. Porosity data from fig. 2

Domain	Number of pores in domain	% of total porosity (%)	Absolute porosity (μm^2)	Porosity presented as % of total area of fig. 1b (%)
Quartz	6991	86	1515	0.07
Porphyroclast + Polyphase	1138	14	247	0.01

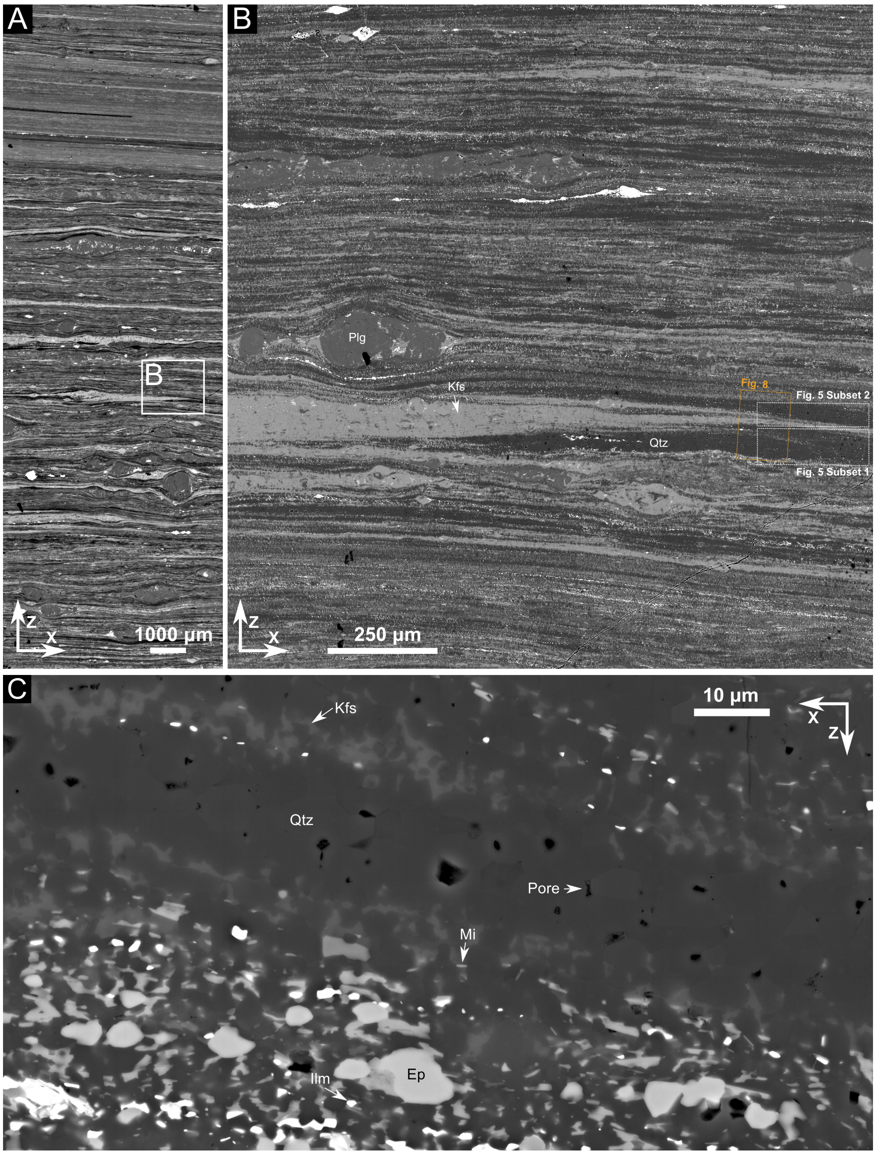

Figure 1. BSE images from the quartzo-feldspathic ultramylonite. Fig. 1a shows the overall strain gradient in the sample, with the highest strain domain found at the top of the image. Fig. 1b is a high-resolution BSE SEM mosaic of a representative area of the sample (41448 x 40282 pixels, scale of 1 px : 35.5 nm). All results presented for pore shape and orientation analysis are from the area of fig. 1b. The greyscale values identify minerals as follows: black = Porosity, dark grey = Qtz, grey= Plg, light grey = Kfs, bright = accessory phases. Fig. 1c presents the edge of a disaggregating quartz domain and highlights the minerals present in the poorly mixed polyphase domains.

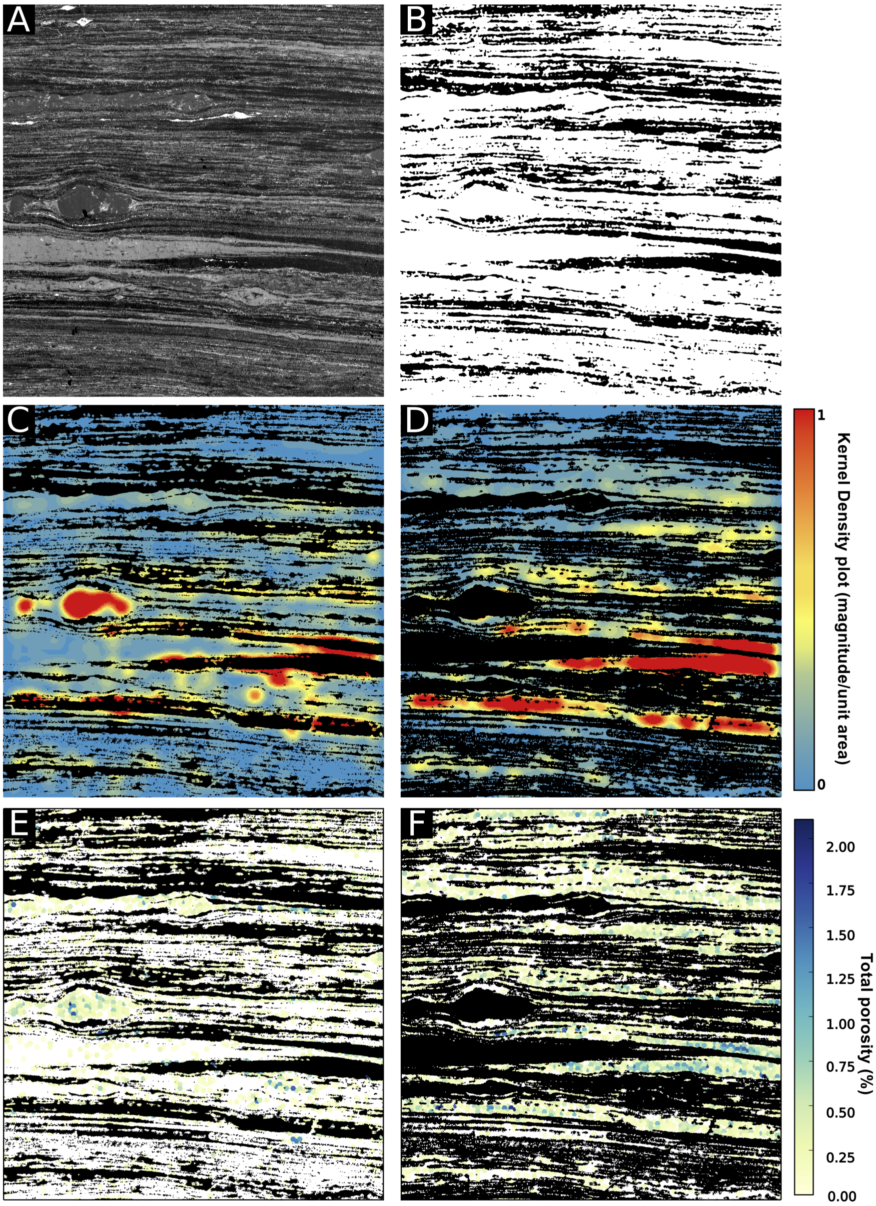

Figure 2. The spatial distribution of porosity in figure 1b. In the BSE mosaic of fig. 1b, 8129 individual pores were identified. For reference, fig. 2a displays the micro-fabric of the area analysed. Fig. 2b is the mask used for distinguishing microstructural domains for analysis: quartz is coloured black. Fig. 2c and d present masked kernel density analysis, highlighting regions of pore clustering. Fig. 2c is masked to remove all quartz and fig. 2d is masked to only show the quartz. The clustering of pores is most prevalent in the thickest, most coherent quartz domains and in the largest feldspar porphyroclasts. Fig. 2e and f are hexbin plots that are coloured to show the absolute porosity per hexbin (masked in the same fashion as fig. 2c and d). See Table 1 for porosity values per domain.

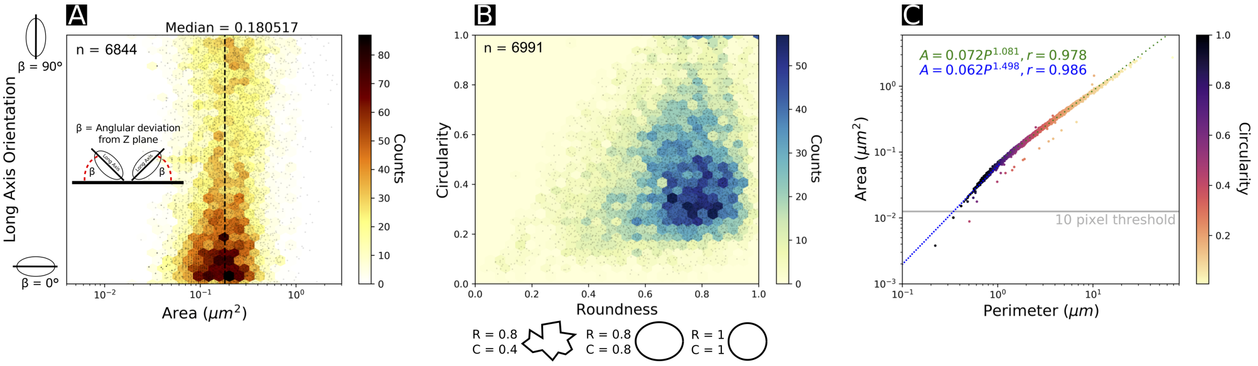

Figure 3. Plots of relationships in pore shape, size and orientation for all pores observed in association with the quartz domains of fig. 1b. Due to the large sample size, pertinent clustering in data is more clearly observed when presented in hexbin plots (actual data points are overlain). In figs. 3a and b, the hexbin plot colouring displays the number of data points contained within each hexbin. Fig. 3a presents area as a function of pore long axis orientation (β = 0° is parallel to the Z plane of finite strain and β = 90° is parallel to the X plane of finite strain). Circular pores (circ = 1) are excluded from fig. 3a because the long of a circle will not have a unique or meaningful orientation. Fig. 3b compares each pore's circularity with its roundness. One large cluster (circ = 0.3, round = 0.8) and two minor clusters (circ = 1, round = 1; circ = 1, round = 0.8) are observed. Fig. 3c shows the relationship of pore perimeter with increasing cross-sectional area. Each data point is additionally coloured for its circularity. Two power law trends are identified in fig. 3c. See text for further discussion.

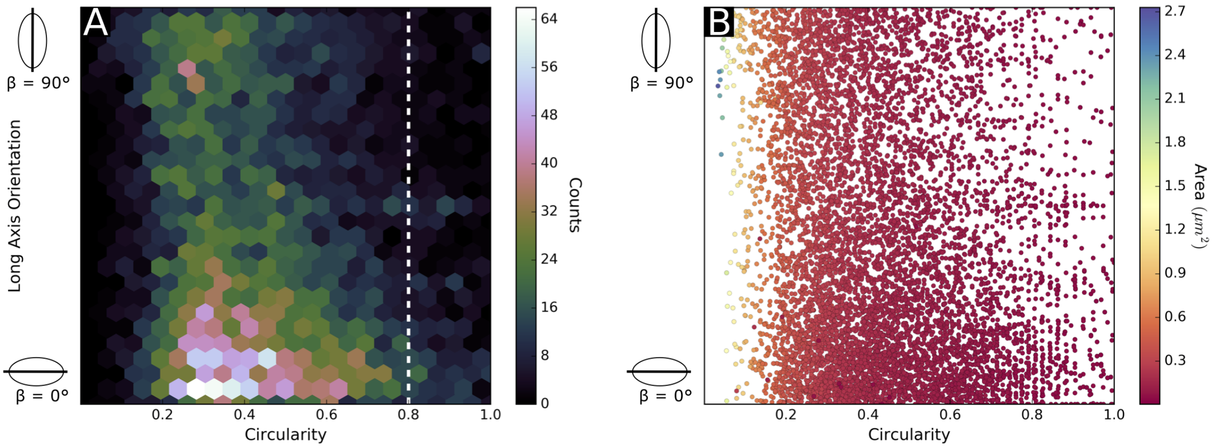

Figure 4. The link between pore orientations, pore sizes and their shapes in detail. Fig. 4 presents only data for pores with circularity values <1. A delineation (circ = 0.8) is presented to show the change in power law relations observed in fig. 3c. Fig. 4a shows that with decreasing circularity there is an increase in the variability of β values. Fig. 4b presents the same data as fig. 4a but with the data points coloured for cross-sectional area. The largest pores are observed to mostly have high β values.

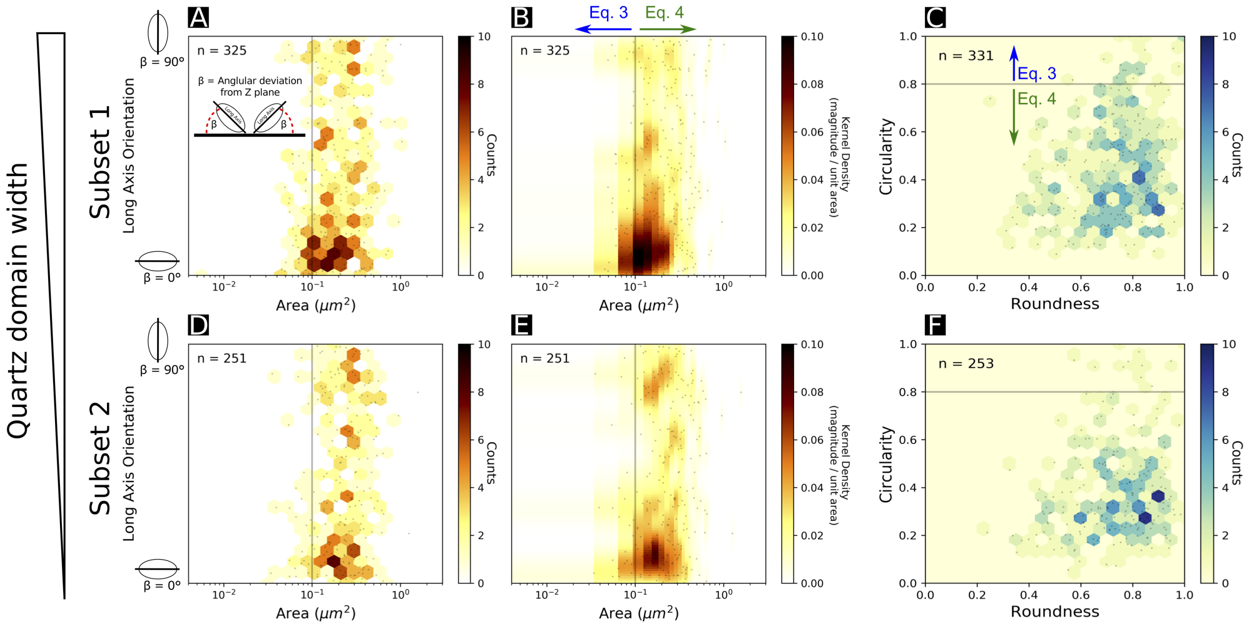

Figure 5. Pore analyses for subsets 1 and 2 shown in fig. 1b, corresponding to decreasing quartz domain width and increasing quartz dispersion. Lines marking the change in pore shape relations described by equations 3 and 4 are presented in each plot. Fig. 5a and d present pore long axis orientation against pore area data in hexbin plots, while fig. 5b and e show the same data but with true point density analysis. Both sets of figures show that with decreasing quartz band thickness, there is an increase in the range of pore orientations observed. Fig. 5c and f demonstrate that this change is also concordant with a change in the pore shapes from roughly elliptical to more complex. More specifically, it can be seen in fig. 5b and d, that with decreasing domain width there is a loss of circular and elliptical pores.

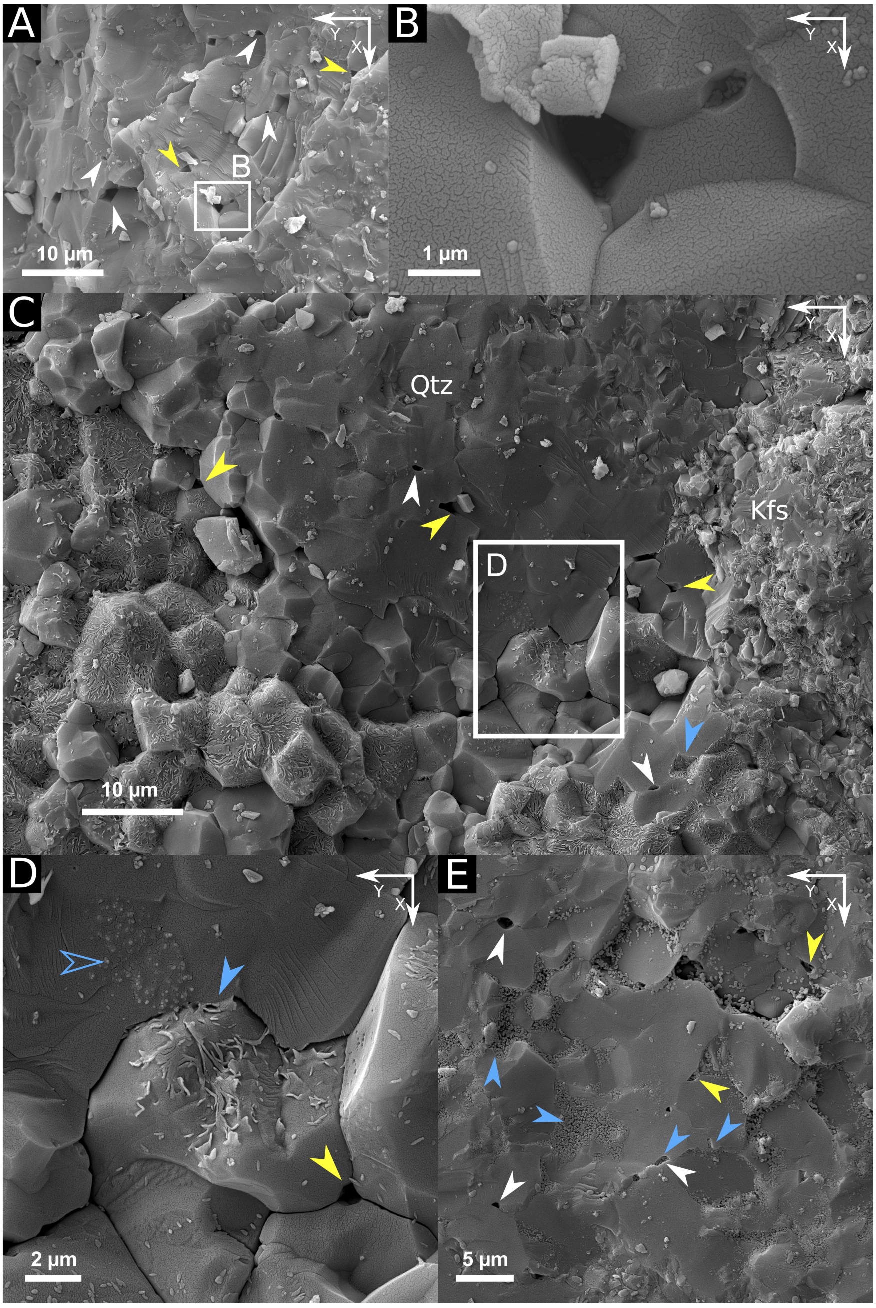

figure.png

Figure 6. Secondary electron images from broken surfaces of quartz domains. White and yellow arrows point, respectively, to pores on grain-boundaries with a low angle to the YZ plane of finite strain and to pores at grain boundary trip junctions. Blue arrows highlight 'precipitation' features, with the empty blue arrow in fig. 6d identifying crystallites interpreted to be incipient precipitates found on a less dilatant grain boundary. Fig. 6a shows a thick, coherent, monomineralic quartz domain that has an abundance of pores. Fig. 6b highlights the difference between a pore found at a triple junction and a pore found in the middle of a grain boundary (see fig. 1c for comparison in XZ plane). Fig. 6c, d and e show the change in porosity and grain boundary features with increasing distance from a plagioclase porphyroclast (see text for more detail).

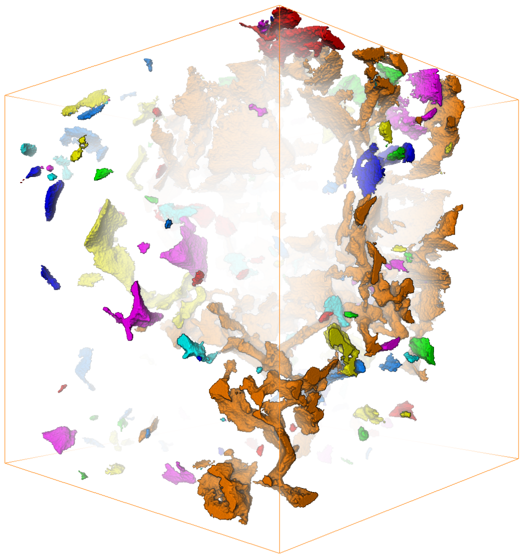

Figure 7. 3-dimensional rendering of cavities segmented from a nanotomographic dataset. Pores are coloured individually to highlight connectivity.. This means that a single colour allows for the tracing out of pore connections. For example, note the large interconnected pore cluster in orange. Dimension of the cube is 700 $voxel^3$, with a voxel size of ∼35 nm. The top and base of the cube are parallel to the mylonitic foliation. The figure indicates the oblate shape of most cavities and proves that they are indeed 3-dimensional features.

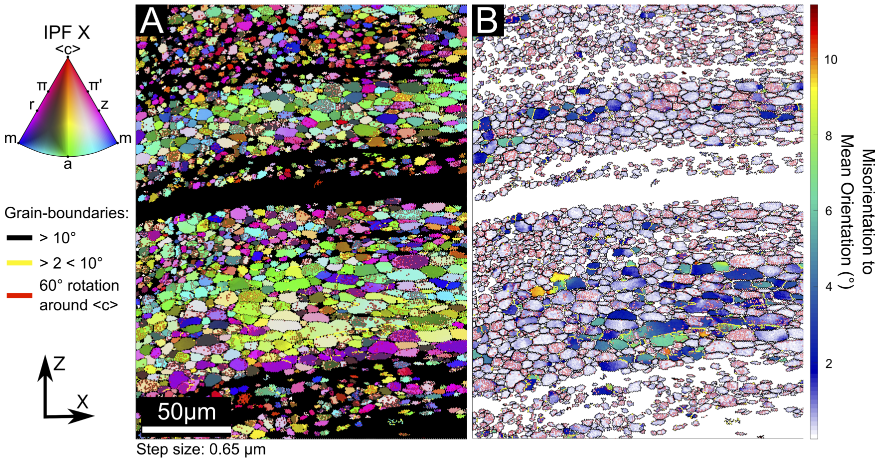

Figure 8. EBSD maps for region of interest in fig. 1b. Fig. 8a shows an inverse pole figure map coloured for the X direction of finite strain. Colours in fig. 8b relate each pixel's orientaiton to the mean orientaiton of the grain that hosts the pixel.

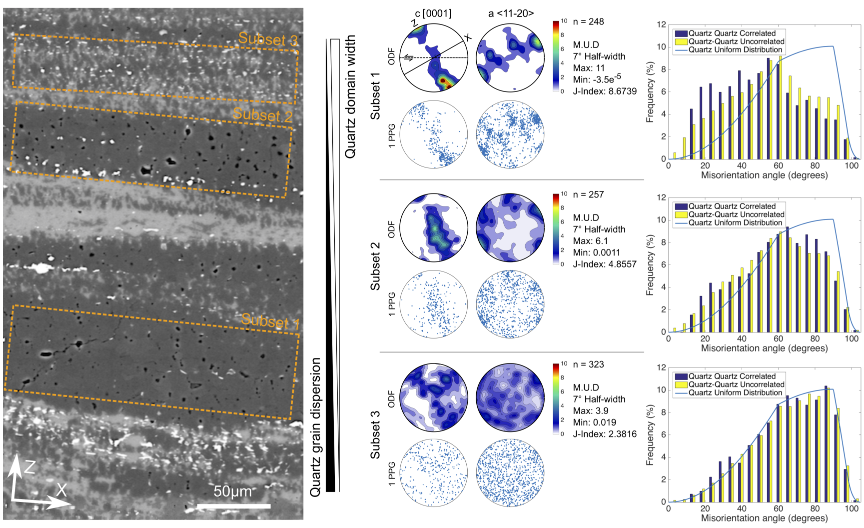

Figure 9. EBSD subset analyses of quartz domains. The EBSD analyses were preformed in the same quartz bands used for subset image analysis (see fig. 1 and 5). EBSD data are presented in equivalent subsets corresponding to decreasing quartz domain width and increasing quartz dispersion. A clear CPO is observed in the pole figure analysis of subset 1 with two c[0001] maxima and two corresponding a<11-20> maxima. As quartz domain thickness decreases there is a randomisation of the CPO, highlighted by the decrease in the J-Index and supported by the shift to a near random distribution of the misorientation angle histogram of subset 3. Note that only grain boundary data are presented in the misorientation angle histograms. Subgrains and Dauphine twin boundaries are excluded from the visualisation.

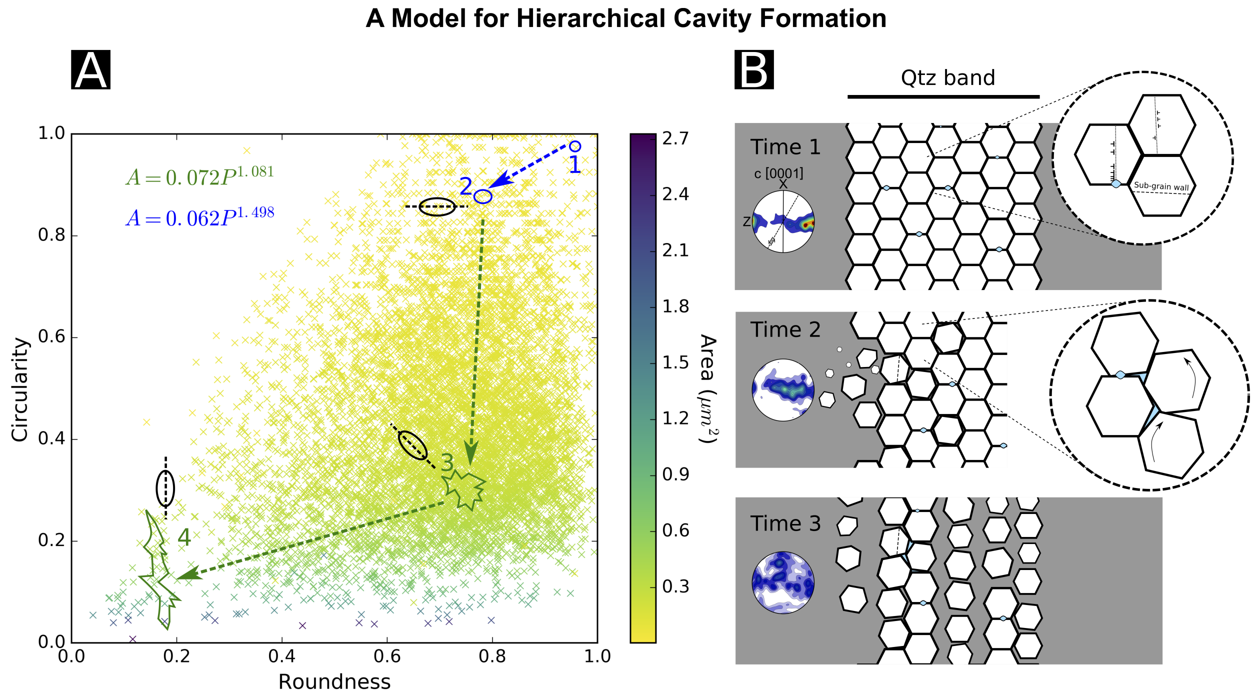

Figure 10. A model for synkinematic creep cavity formation by two different mechanism. Fig. 10a graphically represents the inferred trajectory of a creep cavity's life cycle. Initially creep cavities grow from circular (1) to elliptical cavities (2). These cavities generally have long axes aligned in the Z direction (when viewed in the XZ plane). As cavities become larger they develop more complex shapes and rotate (3), ultimately elongating and becoming more aligned with the shear plane (4). Fig. 10b schematically integrates our observations of cavity evolution with the evolution of the microstructure and the associated micro-mechanisms. First cavities form, in quartz domains deforming by GSI creep, by the Zener-Stroh mechanism (fig. 10b, Time 1). As the grain boundary strength is weakened by the ingress of fluids into cavities, VGBS is promoted. This increase in the contribution of VGBS drives the production of new creep cavities of a more complex shape (fig. 10b, Time 2). It is the production of creep cavities that initiates the increased contribution of VGBS and ultimately prompts a switch to a GSS creep. See text for details.

Competing interests. No competing interests are present

Acknowledgements. We would like to thank Nicola Cayzer (Edinburgh Materials and Micro-Analysis Centre) and Natasha Stephen (Plymouth Electron Microscopy Centre) for their help with the acquisition of SEM data. James Gilgannon would like to thank Marco Herwegh for invaluable discussions about Zener pinning, Cees-Jan De Hoog for council on fluids and phase precipitation, and finally Alfons Berger for EBSD procurement. We kindly thank the reviewers, Jacques Précigout and Luiz F.G. Morales, for their helpful reviews. This work was financially supported by the School of Geosciences, University of Edinburgh. Use of the Advanced Photon Source at Argonne National Laboratory was supported by the U.S. Department of Energy, Office of Science, Office of Basic Energy Sciences, under Contract No. DE-AC02-06CH11357.

References

References

Bauer, R. and Wilsdorf, H.: Void initiation in ductile fracture, Scripta Metallurgica, 7, 1213 – 1220, https://doi.org/10.1016/0036-9748(73)90250-0, http://www.sciencedirect.com/science/article/pii/0036974873902500, 1973.

Behrmann, J.: Crystal plasticity and superplasticity in quartzite; A natural example, Tectonophysics, 115, 101 – 129, https://doi.org/10.1016/0040-1951(85)90102-7, http://www.sciencedirect.com/science/article/pii/0040195185901027, 1985.

Behrmann, J. and Mainprice, D.: Deformation mechanisms in a high-temperature quartz-feldspar mylonite: evidence for superplastic flow in the lower continental crust, Tectonophysics, 140, 297 – 305, https://doi.org/10.1016/0040-1951(87)90236-8, http://www.sciencedirect.com/science/article/pii/0040195187902368, 1987.

Billia, M. A., Timms, N. E., Toy, V. G., Hart, R. D., and Prior, D. J.: Grain boundary dissolution porosity in quartzofeldspathic ultramylonites: Implications for permeability enhancement and weakening of mid-crustal shear zones, Journal of Structural Geology, 53, 2 – 14, https://doi.org/10.1016/j.jsg.2013.05.004, http://www.sciencedirect.com/science/article/pii/S0191814113000850, 2013.

Caristan, Y.: The transition from high temperature creep to fracture in Maryland diabase, Journal of Geophysical Research: Solid Earth, 87, 6781–6790, https://doi.org/10.1029/JB087iB08p06781, http://onlinelibrary.wiley.com/doi/10.1029/JB087iB08p06781/abstract, 1982.

Cox, E. P.: A Method of Assigning Numerical and Percentage Values to the Degree of Roundness of Sand Grains, Journal of Paleontology, 1, 179 –183, http://www.jstor.org/stable/1298056, 1927.

Delle Piane, C., Wilson, C., and Burlini, L.: Dilatant plasticity in high-strain experiments on calcite–muscovite aggregates, Journal of Structural Geology, 31, 1084 – 1099, https://doi.org/10.1016/j.jsg.2009.03.005, http://www.sciencedirect.com/science/article/pii/S019181410900042X, 2009.

Dimanov, A., Rybacki, E., Wirth, R., and Dresen, G.: Creep and strain-dependent microstructures of synthetic anorthite–diopside aggregates, Journal of Structural Geology, 29, 1049 – 1069, https://doi.org/10.1016/j.jsg.2007.02.010, http://www.sciencedirect.com/science/article/pii/S0191814107000338, 2007.

Etheridge, M. and Wilkie, J.: Grainsize reduction, grain boundary sliding and the flow strength of mylonites, Tectonophysics, 58, 159 – 178, https://doi.org/10.1016/0040-1951(79)90327-5, http://www.sciencedirect.com/science/article/pii/0040195179903275, 1979.

Etheridge, M. A., Wall, V. J., Cox, S. F., and Vernon, R. H.: High fluid pressures during regional metamorphism and deformation: Implications for mass transport and deformation mechanisms, Journal of Geophysical Research: Solid Earth, 89, 4344–4358, https://doi.org/10.1029/JB089iB06p04344, http://onlinelibrary.wiley.com/doi/10.1029/JB089iB06p04344/abstract, 1984.

Fliervoet, T. F., White, S. H., and Drury, M. R.: Evidence for dominant grain-boundary sliding deformation in greenschist- and amphibolite-grade polymineralic ultramylonites from the Redbank Deformed Zone, Central Australia, Journal of Structural Geology, 19, 1495 – 1520, https://doi.org/10.1016/S0191-8141(97)00076-X, http://www.sciencedirect.com/science/article/pii/S019181419700076X, 1997.

Fusseis, F., Handy, M., and Schrank, C.: Networking of shear zones at the brittle-to-viscous transition (Cap de Creus, NE Spain), Journal of Structural Geology, 28, 1228 – 1243, https://doi.org/10.1016/j.jsg.2006.03.022, http://www.sciencedirect.com/science/article/pii/S0191814106000757, 2006.

Fusseis, F., Regenauer-Lieb, K., Liu, J., Hough, R. M., and De Carlo, F.: Creep cavitation can establish a dynamic granular fluid pump in ductile shear zones, Nature, 459, 974–977, https://www.nature.com/nature/journal/v459/n7249/full/nature08051.html, 2009.

Gandhi, C. and Ashby, M.: Overview no. 5: Fracture-mechanism maps for materials which cleave: f.c.c., b.c.c. and h.c.p. metals and ceramics, Acta Metallurgica, 27, 1565 – 1602, https://doi.org/10.1016/0001-6160(79)90042-7, http://www.sciencedirect.com/science/article/pii/0001616079900427, 1979.

Handy, M. R.: Flow laws for rocks containing two non-linear viscous phases: A phenomenological approach, Journal of Structural Geology, 16, 287 – 301, https://doi.org/10.1016/0191-8141(94)90035-3, http://www.sciencedirect.com/science/article/pii/0191814194900353, 1994.

Herwegh, M. and Jenni, A.: Granular flow in polymineralic rocks bearing sheet silicates: new evidence from natural examples, Tectonophysics, 332, 309 – 320, https://doi.org/10.1016/S0040-1951(00)00288-2, http://www.sciencedirect.com/science/article/pii/S0040195100002882, 2001.

Herwegh, M., Linckens, J., Ebert, A., Berger, A., and Brodhag, S.: The role of second phases for controlling microstructural evolution in polymineralic rocks: A review, Journal of Structural Geology, 33, 1728 – 1750, https://doi.org/10.1016/j.jsg.2011.08.011, http://www.sciencedirect.com/science/article/pii/S0191814111001416, 2011.

Herwegh, M., Poulet, T., Karrech, A., and Regenauer-Lieb, K.: From transient to steady state deformation and grain size: A thermodynamic approach using elasto-visco-plastic numerical modeling, Journal of Geophysical Research: Solid Earth, 119, 900–918, https://doi.org/10.1002/2013JB010701, http://onlinelibrary.wiley.com/doi/10.1002/2013JB010701/abstract, 2013JB010701, 2014.

Hippertt, J. F. M.: Grain Boundary Microstructures in Micaceous Quartzite: Significance for Fluid Movement and Deformation Processes in Low Metamorphic Grade Shear Zones, The Journal of Geology, 102, 331–348, https://doi.org/10.1086/629675, http://www.journals.uchicago.edu/doi/10.1086/629675, 1994.

Hirth, G. and Tullis, J.: The effects of pressure and porosity on the micromechanics of the brittle-ductile transition in quartzite, Journal of Geophysical Research: Solid Earth, 94, 17 825–17 838, https://doi.org/10.1029/JB094iB12p17825, http://onlinelibrary.wiley.com/doi/10.1029/JB094iB12p17825/full, 1989.

Huang, M., Rivera-Díaz-del-Castillo, P. E. J., Bouaziz, O., and van der Zwaag, S.: Modelling the steady state deformation stress under various deformation conditions using a single irreversible thermodynamics based formulation, Acta Materialia, 57, 3431 – 3438, https://doi.org/10.1016/j.actamat.2009.03.023, http://www.sciencedirect.com/science/article/pii/S1359645409001748, 2009.

Hunter, J. D.: Matplotlib: A 2D graphics environment, Computing In Science & Engineering, 9, 90–95, https://doi.org/10.1109/MCSE.2007.55, http://aip.scitation.org/doi/abs/10.1109/MCSE.2007.55?journalCode=csx, 2007.

Ingebritsen, S. E. and Manning, C. E.: Permeability of the continental crust: dynamic variations inferred from seismicity and metamorphism, Geofluids, 10, 193–205, https://doi.org/10.1111/j.1468-8123.2010.00278.x, http://onlinelibrary.wiley.com/doi/10.1111/j.1468-8123.2010.00278.x/abstract, 2010.

Jones, E., Oliphant, T., Peterson, P., et al.: SciPy: Open source scientific tools for Python, http://www.scipy.org/, 2001–.

Kerrich, R., Allison, I., Barnett, R. L., Moss, S., and Starkey, J.: Microstructural and chemical transformations accompanying deformation of granite in a shear zone at Miéville, Switzerland; with implications for stress corrosion cracking and superplastic flow, Contributions to Mineralogy and Petrology, 73, 221–242, https://doi.org/10.1007/BF00381442, https://link.springer.com/article/10.1007%2FBF00381442, 1980.

Kilian, R., Heilbronner, R., and Stünitz, H.: Quartz grain size reduction in a granitoid rock and the transition from dislocation to diffusion creep, Journal of Structural Geology, 33, 1265 – 1284, https://doi.org/10.1016/j.jsg.2011.05.004, http://www.sciencedirect.com/science/article/pii/S0191814111000848, 2011.

Kruse, R. and Stünitz, H.: Deformation mechanisms and phase distribution in mafic high-temperature mylonites from the Jotun Nappe, southern Norway, Tectonophysics, 303, 223 – 249, https://doi.org/10.1016/S0040-1951(98)00255-8, http://www.sciencedirect.com/science/article/pii/S0040195198002558, 1999.

Mainprice, D., Hielscher, R., and Schaeben, H.: Calculating anisotropic physical properties from texture data using the MTEX open-source package, Geological Society, London, Special Publications, 360, 175–192, https://doi.org/10.1144/SP360.10, http://sp.lyellcollection.org/content/360/1/175, 2011.

Mancktelow, S. N., Grujic, D., and Johnson, L. E.: An SEM study of porosity and grain boundary microstructure in quartz mylonites, Simplon Fault Zone, Central Alps, Contributions to Mineralogy and Petrology, 131, 71–85, https://doi.org/10.1007/s004100050379, https://link.springer.com/article/10.1007/s004100050379, 1998.

Menegon, L., Fusseis, F., Stünitz, H., and Xiao, X.: Creep cavitation bands control porosity and fluid flow in lower crustal shear zones, Geology, 43, 227–230, https://doi.org/10.1130/G36307.1, http://geology.gsapubs.org/content/43/3/227.abstract, 2015.

Mitra, G.: Ductile deformation zones and mylonites; the mechanical processes involved in the deformation of crystalline basement rocks, American Journal of Science, 278, 1057–1084, https://doi.org/10.2475/ajs.278.8.1057, http://www.ajsonline.org/content/278/8/1057.short, 1978.

Paterson, M. S.: A theory for granular flow accommodated by material transfer via an intergranular fluid, Tectonophysics, 245, 135 – 151, https://doi.org/10.1016/0040-1951(94)00231-W, http://www.sciencedirect.com/science/article/pii/004019519400231W, 1995.

Peters, M., Veveakis, M., Poulet, T., Karrech, A., Herwegh, M., and Regenauer-Lieb, K.: Boudinage as a material instability of elasto-visco-plastic rocks, Journal of Structural Geology, 78, 86–102, https://doi.org/10.1016/j.jsg.2015.06.005, http://www.sciencedirect.com/science/article/pii/S0191814115300043, 2015.

Poirier, J.: Shear zones in rocks Shear localization and shear instability in materials in the ductile field, Journal of Structural Geology, 2, 135 – 142, https://doi.org/10.1016/0191-8141(80)90043-7, http://www.sciencedirect.com/science/article/pii/0191814180900437, 1980.

Précigout, J. and Stünitz, H.: Evidence of phase nucleation during olivine diffusion creep: A new perspective for mantle strain localisation, Earth and Planetary Science Letters, 455, 94 – 105, https://doi.org/10.1016/j.epsl.2016.09.029, http://www.sciencedirect.com/science/article/pii/S0012821X1630509X, 2016.

Précigout, J., Prigent, C., Palasse, L., and Pochon, A.: Water pumping in mantle shear zones, Nature Communications, 8, https://doi.org/110.1038/ncomms15736, https://www.nature.com/articles/ncomms15736, 2017.

Ree, J.-H.: Grain boundary sliding and development of grain boundary openings in experimentally deformed octachloropropane, Journal of Structural Geology, 16, 403 – 418, https://doi.org/10.1016/0191-8141(94)90044-2, http://www.sciencedirect.com/science/article/pii/0191814194900442, 1994.

Riedel, H.: Fracture at high temperatures, Springer, 1987.

Rogowitz, A., White, J. C., and Grasemann, B.: Strain localization in ultramylonitic marbles by simultaneous activation of dislocation motion and grain boundary sliding (Syros, Greece), Solid Earth, 7, 355–366, https://doi.org/10.5194/se-7-355-2016, http://www.solid-earth.net/7/355/2016/, 2016.

Rovetta, M. R., Delaney, J. R., and Blacic, J. D.: A record of high-temperature embrittlement of peridotite in CO2 permeated xenoliths from basalt, Journal of Geophysical Research: Solid Earth, 91, 3841–3848, https://doi.org/10.1029/JB091iB03p03841, http://onlinelibrary.wiley.com/doi/10.1029/JB091iB03p03841/full, 1986.

Rybacki, E., Wirth, R., and Dresen, G.: High-strain creep of feldspar rocks: Implications for cavitation and ductile failure in the lower crust, Geophysical Research Letters, 35, n/a–n/a, https://doi.org/10.1029/2007GL032478, http://onlinelibrary.wiley.com/doi/10.1029/2007GL032478/abstract, l04304, 2008.

Schindelin, J., Arganda-Carreras, I., Frise, E., Kaynig, V., Longair, M., Pietzsch, T., Preibisch, S., Rueden, C., Saalfeld, S., Schmid, B., Tinevez, J.-Y., White, D. J., Hartenstein, V., Eliceiri, K., Tomancak, P., and Cardona, A.: Fiji: an open-source platform for biological-image analysis, Nat Meth, 9, 676–682, https://doi.org/10.1038/nmeth.2019, https://www.nature.com/nmeth/journal/v9/n7/full/nmeth.2019.html, 2012.

Shigematsu, N., Fujimoto, K., Ohtani, T., and Goto, K.: Ductile fracture of fine-grained plagioclase in the brittle–plastic transition regime: implication for earthquake source nucleation, Earth and Planetary Science Letters, 222, 1007 – 1022, https://doi.org/10.1016/j.epsl.2004.04.001, http://www.sciencedirect.com/science/article/pii/S0012821X04002365, 2004.

Smith, R.: Unified theory of the onset of folding, boudinage, and mullion structure, Geological Society of America Bulletin, 86, 1601–1609, https://doi.org/10.1130/0016-7606(1975)86<1601:UTOTOO>2.0.CO;2, http://gsabulletin.gsapubs.org/content/86/11/1601, 1975.

Stipp, M., Stünitz, H., Heilbronner, R., and Schmid, S. M.: The eastern Tonale fault zone: a ‘natural laboratory’ for crystal plastic deformation of quartz over a temperature range from 250 to 700C, Journal of Structural Geology, 24, 1861 – 1884, https://doi.org/10.1016/S0191-8141(02)00035-4, http://www.sciencedirect.com/science/article/pii/S0191814102000354, 2002.

Stroh, A.: A theory of the fracture of metals, Advances in Physics, 6, 418–465, https://doi.org/10.1080/00018735700101406, http://www.tandfonline.com/doi/abs/10.1080/00018735700101406, 1957.

Teyssier, C.: High strain zones in the continental crust: the central Australian example, Ph.D. thesis, 1985a.

Teyssier, C.: A crustal thrust system in an intracratonic tectonic environment, Journal of Structural Geology, 7, 689 – 700, https://doi.org/10.1016/0191-8141(85)90144-0, http://www.sciencedirect.com/science/article/pii/0191814185901440, 1985b.

Tullis, J.: Deformation of Granitic Rocks: Experimental Studies and Natural Examples, Reviews in Mineralogy and Geochemistry, 51, 51–95, https://doi.org/10.2138/gsrmg.51.1.51, http://rimg.geoscienceworld.org/content/51/1/51, 2002.

van der Walt, S., Colbert, S. C., and Varoquaux, G.: The NumPy Array: A Structure for Efficient Numerical Computation, Computing in Science Engineering, 13, 22 – 30, https://doi.org/10.1109/MCSE.2011.37, http://ieeexplore.ieee.org/document/5725236/, 2011.

Viegas, G., Menegon, L., and Archanjo, C.: Brittle grain-size reduction of feldspar, phase mixing and strain localization in granitoids at mid-crustal conditions (Pernambuco shear zone, NE Brazil), Solid Earth, 7, 375–396, https://doi.org/10.5194/se-7-375-2016, https://www.solid-earth.net/7/375/2016/, 2016.

Wintsch, R. P. and Dunning, J.: The effect of dislocation density on the aqueous solubility of quartz and some geologic implications: A theoretical approach, Journal of Geophysical Research: Solid Earth, 90, 3649–3657, https://doi.org/10.1029/JB090iB05p03649, http://onlinelibrary.wiley.com/doi/10.1029/JB090iB05p03649/abstract, 1985.

Wong, T.-F.: A note on the propagation behavior of a crack nucleated by a dislocation pileup, Journal of Geophysical Research: Solid Earth, 95, 8639–8646, https://doi.org/10.1029/JB095iB06p08639, http://onlinelibrary.wiley.com/doi/10.1029/JB095iB06p08639/abstract, 1990.

Závada, P., Schulmann, K., Konopásek, J., Ulrich, S., and Lexa, O.: Extreme ductility of feldspar aggregates—Melt-enhanced grain boundary sliding and creep failure:Rheological implications for felsic lower crust, Journal of Geophysical Research: Solid Earth, 112, n/a–n/a, https://doi.org/10.1029/2006JB004820, http://onlinelibrary.wiley.com/doi/10.1029/2006JB004820/abstract, b10210, 2007.